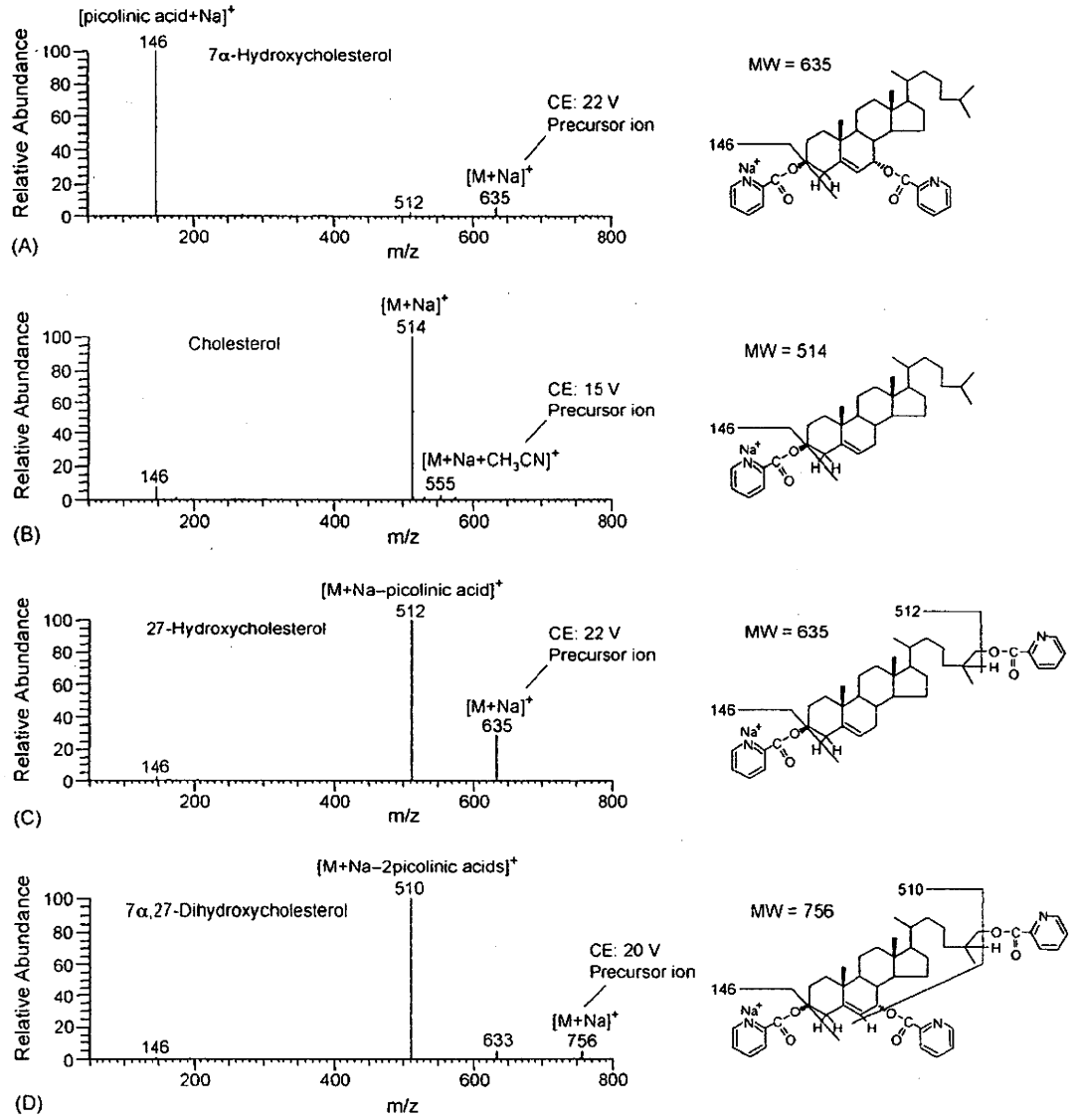

Fig. 2. Representative positive ESI-MS/MS fragmentation patterns of the picolinyl ester derivatives of sterols. (A) 7α-hydroxycholesterol, (B) cholesterol, (C) 27-hydroxycholesterol, (D) 7α,27-dihydroxycholesterol. $[M+Na]^+$ was used as precursor ions for A, C and D, while $[M+Na+CH_3CN]^+$ was used as a precursor ion for B. Fragmentation patterns of A, B, C and D correspond to those in Table 2. The general LC–MS/MS conditions were as follows: introducing solvent, acetonitrile–methanol–water (45:45:10, v/v/v) containing 0.1% acetic acid; flow rate, 300 μl/min; spray voltage, 1000 V. CE, collision energy. In the case of oxysterols with multiple hydroxyl groups (A, C and D), the position of sodium in the picolinyl derivatives has not been determined. In structural formulae, sodium ion was tentatively added to picolinyl group at the C-3β position.

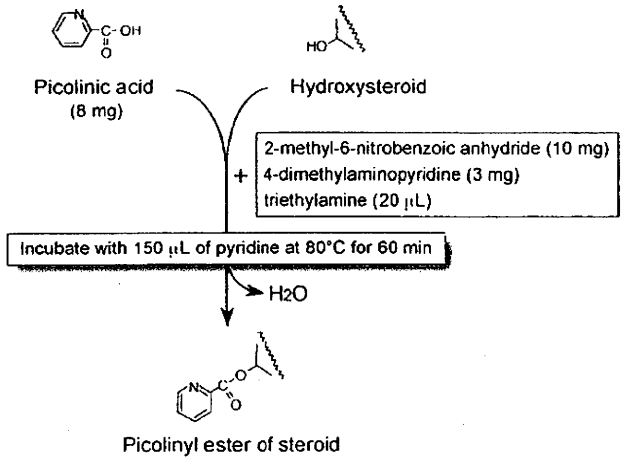

Fig. 3. The formation of picolinyl ester derivative and the conditions of the reaction.

Transesterification of fatty acyl esters during the formation of picolinyl esters is another possibility for the overestimation of sterols. However, the incubation of pure cholesteryl stearate in the reaction mixture showed that the transesterification was not probable.

4.4. Chromatographic separation

HPLC is performed using a reversed-phase Hypersil GOLD column (150 mm × 2.1 mm I.D., 3 μm, Thermo Fisher Scientific, San Jose, CA, USA). In our previous reports, monohydroxysterols [43] and oxysterols [44] were measured separately, but both sterols can be analyzed simultaneously because the HPLC column and gradient conditions are the same. Initially, the mobile phase is comprised of acetonitrile–methanol–water (40:40:20, v/v/v) containing 0.1% acetic acid, and it is then programmed in a linear manner to acetonitrile–methanol–water (45:45:10, v/v/v) containing 0.1% acetic acid over 20 min. The final mobile phase is

Please cite this article in press as: A. Honda, et al., Highly sensitive and specific analysis of sterol profiles in biological samples by HPLC–ESI–MS/MS, J. Steroid Biochem. Mol. Biol. (2010), doi:10.1016/j.jsbmb.2010.03.030

maintained constant for an additional 20 min. The flow rate is 300 μl/min, and the column is maintained at 40 °C using a column oven.

Relative retention times (RRTs), expressed relative to the retention time of cholesterol, are listed in Table 2. The RRTs show that the separation of sterols by the Hypersil GOLD column is excellent, but several weak points are also indicated. First, 7β-hydroxycholesterol gives a peak just before 7α-hydroxycholesterol, and reliable quantification of each hydroxycholesterol can occasionally be difficult. Second, the retention times of 7α-hydroxy-4-cholesten-3-one and 24S,25-epoxycholesterol are very close to each other, and ~~therefore, both peaks are not differentiated~~. However, because 7α-hydroxy-4-cholesten-3-one does not survive alkaline hydrolysis, the peak detected after alkaline hydrolysis is 24S,25-epoxycholesterol alone. Third, lanosterol gives a peak just after cholesterol. Although the monitoring ion for lanosterol is different from that for cholesterol, a huge cholesterol peak in biological samples can sometimes interfere with the lanosterol peak.

These problems are resolved by using another reversed-phase column, Hypersil GOLD aQ (150 mm × 2.1 mm I.D., 3 μm, Thermo Fisher Scientific). This column is usually used for separations employing highly aqueous mobile phases, but we use it as follows: initially, the mobile phase is comprised of acetonitrile–methanol–water (40:40:20, v/v/v) containing 0.1% acetic acid; it is then programmed in a linear manner to acetonitrile–methanol (50:50, v/v) containing 0.1% acetic acid over 40 min. The final mobile phase is maintained constant for an additional 2 min. The flow rate is 300 μl/min, and the column is maintained at 40 °C using a column oven.

The RRTs by the Hypersil GOLD aQ column are also shown in Table 2. Compared with the Hypersil GOLD column, the width of each peak tends to be wide, and the order of elution from the column is very different. Good chromatographic separations are achieved between 7α-hydroxycholesterol and 7β-hydroxycholesterol, 7α-hydroxy-4-cholesten-3-one and 24S,25-epoxycholesterol, and cholesterol and lanosterol. However, the lathosterol and 8-lathosterol peaks are not differentiated.

The separations of picolinylated sterols by these reversed-phase columns are not at all inferior to the separation of free sterols by reversed-phase HPLC [15,21]. For example, the separation of 24-hydroxycholesterol and 25-hydroxycholesterol was difficult, but DeBarber et al. achieved the chromatographic separation and quantification by using a mobile phase consisted of acetonitrile–methanol–water and APCI-MS/MS detector [33]. In contrast, McDonald et al. failed to quantify these sterol isomers separately by using an eluent of methanol–water and ESI-MS/MS detector [21]. They did not use acetonitrile because the presence of acetonitrile significantly reduced signal intensity of sterols analyzed by this detector. As for picolinylated 24- and 25-hydroxycholesterols, they were well separated each other by using acetonitrile–methanol–water as a mobile phase, and excellent sensitivities were achieved by ESI–MS/MS detector.

4.5. Sample preparation

Long term storage or repeated freeze and thaw of biological samples should be avoided because it stimulates cholesterol autoxidation [61]. Addition of the antioxidant, butylated hydroxytoluene, to the sample before sample preparation produced only a modest decrease in oxidation. Therefore, minimizing oxidation by using good lab practices is important [21].

To analyze the unesterified fraction of sterols, serum (1–5 μl), subcellular fraction of tissue (0.1–1.0 mg protein), or cell homogenate (1×10^4–1×10^5 cells) is dried with the added internal standards, and directly derivatized to the picolinyl esters [43]. To analyze the total (unesterified + esterified) fraction, saponification is carried out in 1 N ethanolic KOH at 37 °C for 1 h, and sterols are extracted with *n*-hexane before derivatization [44]. It may be mentioned here that some sterols occur as conjugates with sulfuric or glucuronic acid [62–64]. Negative ESI mode without derivatization is suitable for the analyses of these conjugated sterols, and the conjugated sterols are much more polar than picolinyl esters of unconjugated sterols.

Because this assay method is very sensitive, we can minimize the loading of derivatized sample on the HPLC column. Although the solid-phase extraction/purification step is omitted, target sterols are successfully separated by the HPLC–MS/MS step. In case of human serum analysis, less than 1 ng of picolinyl esters of non-cholesterol sterols are injected onto the column with approximately 200 ng of cholesterol picolinate. Under our HPLC conditions, this amount of cholesterol picolinate is easily trapped in the Hypersil GOLD and Hypersil GOLD aQ columns and eluted at around 28.5 min and 36.5 min, respectively, which is well separated from the picolinyl esters of most non-cholesterol sterols.

While picolinyl esters of sterols are very soluble in acetonitrile, nonpolar compounds, such as fatty acyl esters of cholesterol, remain underivatized and do not dissolve in the final acetonitrile solution. Nonpolar compounds are strongly retained on reversed-phase HPLC columns, but in this method, loading of the nonpolar compounds on the column is minimized.

4.6. Precision and accuracy

The linearity of the standard curves, as determined by simple linear regression, was excellent, as reported in our previous papers [43,44]. Reproducibilities and recoveries of some sterols were validated according to a one-way layout and polynomial equation, respectively [43,44]. The variances between sample preparations and between measurements by this method were calculated to be 1.6–12.7% and 2.5–16.5%, respectively. In these results, higher values of the variances (over 10%) were obtained by the quantification of sterols that showed extremely low concentrations in the samples. To test matrix effects, the recovery experiments were performed using human serum or rat liver microsomes spiked with 0.05–12 ng of sterols. Recoveries of the sterols ranged from 86.7% to 107.3% with a mean recovery of 99.3%, which suggests that matrix effects are not significant in this assay. This method provides reproducible and reliable results for the quantification of sterols in small amounts of biological samples.

5. Perspectives

HPLC–MS or HPLC–MS/MS does not require a derivatization step before the analysis of sterols, which is advantageous for a high-throughput assay. However, the addition of the derivatization step has markedly improved the sensitivities of the neutral sterols. Thus, simple and rapid procedures do not always produce good results for the microanalysis of biological samples. In addition, since many sterols have the same molecular weight and similar structures, a thorough chromatographic separation is essential to maintain the selectivity even if the latest model of mass spectrometer is operated in a high-resolution mode.

The recent development of steroid biochemistry has demonstrated that there are considerable bioactive or biomarker sterols among intermediates and their derivatives in the biosynthetic pathways of cholesterol, bile acids and steroid hormones. Moreover, there are still many unidentified sterols in biological samples. Therefore, not only sensitive and specific quantification of targeted sterols but also metabolomic analysis of whole sterol profiles will become an important methodology for steroid biochemistry and its clinical applications.

Please cite this article in press as: A. Honda, et al., Highly sensitive and specific analysis of sterol profiles in biological samples by HPLC–ESI–MS/MS, J. Steroid Biochem. Mol. Biol. (2010), doi:10.1016/j.jsbmb.2010.03.030

References

[1] S. Gill, R. Chow, A.J. Brown, Sterol regulators of cholesterol homeostasis and beyond: the oxysterol hypothesis revisited and revised, Prog. Lipid Res. 47 (2008) 391–404.

[2] I. Björkhem, T. Miettinen, E. Reihner, S. Ewerth, B. Angelin, K. Einarsson, Correlation between serum levels of some cholesterol precursors and activity of HMG-CoA reductase in human liver, J. Lipid Res. 28 (1987) 1137–1143.

[3] H.J. Kempen, J.F. Glatz, J.A. Gevers Leuven, H.A. van der Voort, M.B. Katan, Serum lathosterol concentration is an indicator of whole-body cholesterol synthesis in humans, J. Lipid Res. 29 (1988) 1149–1155.

[4] T.A. Miettinen, R.S. Tilvis, Y.A. Kesäniemi, Serum plant sterols and cholesterol precursors reflect cholesterol absorption and synthesis in volunteers of a randomly selected male population, Am. J. Epidemiol. 131 (1990) 20–31.

[5] I. Björkhem, E. Reihnér, B. Angelin, S. Ewerth, J.-E. Åkerlund, K. Einarsson, On the possible use of the serum level of 7α-hydroxycholesterol as a marker for increased activity of the cholesterol 7α-hydroxylase in humans, J. Lipid Res. 28 (1987) 889–894.

[6] T. Yoshida, A. Honda, N. Tanaka, Y. Matsuzaki, B. He, T. Osuga, N. Kobayashi, K. Ozawa, H. Miyazaki, Simultaneous determination of mevalonate and 7α-hydroxycholesterol in human plasma by gas chromatography–mass spectrometry as indices of cholesterol and bile acid biosynthesis, J. Chromatogr. 613 (1993) 185–193.

[7] G.S. Tint, M. Irons, E.R. Elias, A.K. Batta, R. Frieden, T.S. Chen, G. Salen, Defective cholesterol biosynthesis associated with the Smith–Lemli–Opitz syndrome, N. Engl. J. Med. 330 (1994) 107–113.

[8] D.R. FitzPatrick, J.W. Keeling, M.J. Evans, A.E. Kan, J.E. Bell, M.E. Porteous, K. Mills, R.M. Winter, P.T. Clayton, Clinical phenotype of desmosterolosis, Am. J. Med. Genet. 75 (1998) 145–152.

[9] R.I. Kelley, W.G. Wilcox, M. Smith, L.E. Kratz, A. Moser, D.S. Rimoin, Abnormal sterol metabolism in patients with Conradi–Hunermann–Happle syndrome and sporadic lethal chondrodysplasia punctata, Am. J. Med. Genet. 83 (1999) 213–219.

[10] P.A. Krakowiak, C.A. Wassif, L. Kratz, D. Cozma, M. Kovarova, G. Harris, A. Grinberg, Y. Yang, A.G. Hunter, M. Tsokos, R.I. Kelley, F.D. Porter, Lathosterolosis: an inborn error of human and murine cholesterol synthesis due to lathosterol 5-desaturase deficiency, Hum. Mol. Genet. 12 (2003) 1631–1641.

[11] G. Salen, S. Shefer, L. Nguyen, G.C. Ness, G.S. Tint, V. Shore, Sitosterolemia, J. Lipid Res. 33 (1992) 945–955.

[12] G. Halperin, M. Elisaf, E. Leitersdorf, D. Harats, A new method for determination of serum cholestanol by high-performance liquid chromatography with ultraviolet detection, J. Chromatogr. B Biomed. Sci. Appl. 742 (2000) 345–352.

[13] B.J. Koopman, J.C. van der Molen, B.G. Wolthers, J.B. Vanderpas, Determination of some hydroxycholesterols in human serum samples, J. Chromatogr. 416 (1987) 1–13.

[14] P.B. Hylemon, E.J. Studer, W.M. Pandak, D.M. Heuman, Z.R. Vlahcevic, Y.L. Chiang, Simultaneous measurement of cholesterol 7α-hydroxylase activity by reverse-phase high-performance liquid chromatography using both endogenous and exogenous [4-^{14}C]cholesterol as substrate, Anal. Biochem. 182 (1989) 212–216.

[15] B. Ruan, N. Gerst, G.T. Emmons, J. Shey, G.J. Schroepfer Jr., Sterol synthesis. A timely look at the capabilities of conventional and silver ion high performance liquid chromatography for the separation of C27 sterols related to cholesterol biosynthesis, J. Lipid Res. 38 (1997) 2615–2626.

[16] T. Saldanha, A.C. Sawaya, M.N. Eberlin, N. Bragagnolo, HPLC separation and determination of 12 cholesterol oxidation products in fish: comparative study of RI, UV, and APCI-MS detectors, J. Agric. Food Chem. 54 (2006) 4107–4113.

[17] A. Cohen, H.S. Hertz, J. Mandel, R.C. Paule, R. Schaffer, L.T. Sniegoski, T. Sun, M.J. Welch, V.E. White, Total serum cholesterol by isotope dilution/mass spectrometry: a candidate definitive method, Clin. Chem. 26 (1980) 854–860.

[18] S. Dzeletovic, O. Breuer, E. Lund, U. Diczfalusy, Determination of cholesterol oxidation products in human plasma by isotope dilution-mass spectrometry, Anal. Biochem. 225 (1995) 73–80.

[19] H.S. Ahmida, P. Bertucci, L. Franzo, R. Massoud, C. Cortese, A. Lala, G. Federici, Simultaneous determination of plasmatic phytosterols and cholesterol precursors using gas chromatography–mass spectrometry (GC–MS) with selective ion monitoring (SIM), J. Chromatogr. B Analyt. Technol. Biomed. Life Sci. 842 (2006) 43–47.

[20] J. Lembcke, U. Ceglarek, G.M. Fiedler, S. Baumann, A. Leichtle, J. Thiery, Rapid quantification of free and esterified phytosterols in human serum using APPI-LC–MS/MS, J. Lipid Res. 46 (2005) 21–26.

[21] J.C. McDonald, B.M. Thompson, E.C. McCrum, D.W. Russell, Extraction and analysis of sterols in biological matrices by high performance liquid chromatography electrospray ionization mass spectrometry, Methods Enzymol. 432 (2007) 145–170.

[22] Z. Zhang, D. Li, D.E. Blanchard, S.R. Lear, S.K. Erickson, T.A. Spencer, Key regulatory oxysterols in liver: analysis as Δ^4-3-ketone derivatives by HPLC and response to physiological perturbations, J. Lipid Res. 42 (2001) 649–658.

[23] B. Ruan, W.K. Wilson, J. Pang, N. Gerst, F.D. Pinkerton, J. Tsai, R.I. Kelley, F.G. Whitby, D.M. Milewicz, J. Garbern, G.J. Schroepfer Jr., Sterols in blood of normal and Smith–Lemli–Opitz subjects, J. Lipid Res. 42 (2001) 799–812.

[24] W. Sattler, H.J. Leis, G.M. Kostner, E. Malle, Quantification of 7-dehydrocholesterol in plasma and amniotic fluid by liquid chromatography/particle beam-mass spectrometry as a biochemical diagnostic marker for the Smith–Lemli–Opitz syndrome, Rapid Commun. Mass Spectrom. 9 (1995) 1288–1292.

[25] M. Careri, P. Ferretti, P. Manini, M. Musci, Evaluation of particle beam high-performance liquid chromatography–mass spectrometry for analysis of cholesterol oxides, J. Chromatogr. A 794 (1998) 253–262.

[26] P. Manini, R. Andreoli, M. Careri, L. Elviri, M. Musci, Atmospheric pressure chemical ionization liquid chromatography/mass spectrometry in cholesterol oxide determination and characterization, Rapid Commun. Mass Spectrom. 12 (1998) 883–889.

[27] E. Razzazi-Fazeli, S. Kleineisen, W. Luf, Determination of cholesterol oxides in processed food using high-performance liquid chromatography–mass spectrometry with atmospheric pressure chemical ionization, J. Chromatogr. A 896 (2000) 321–334.

[28] I. Burkard, K.M. Rentsch, A. von Eckardstein, Determination of 24S- and 27-hydroxycholesterol in plasma by high-performance liquid chromatography–mass spectrometry, J. Lipid Res. 45 (2004) 776–781.

[29] J.J. Palmgren, A. Toyras, T. Mauriala, J. Monkkonen, S. Auriola, Quantitative determination of cholesterol, sitosterol, and sitostanol in cultured Caco-2 cells by liquid chromatography-atmospheric pressure chemical ionization mass spectrometry, J. Chromatogr. B Analyt. Technol. Biomed. Life Sci. 821 (2005) 144–152.

[30] K. Raith, C. Brenner, H. Farwanah, G. Müller, K. Eder, R.H.H. Neubert, A new LC/APCI-MS method for the determination of cholesterol oxidation products in food, J. Chromatogr. A 1067 (2005) 207–211.

[31] K. Nagy, A. Jakab, F. Pollreisz, D. Bongiorno, L. Ceraulo, M.R. Averna, D. Noto, K. Vekey, Analysis of sterols by high-performance liquid chromatography/mass spectrometry combined with chemometrics, Rapid Commun. Mass Spectrom. 20 (2006) 2433–2440.

[32] Q. Tian, M.L. Failla, T. Bohn, S.J. Schwartz, High-performance liquid chromatography/atmospheric pressure chemical ionization tandem mass spectrometry determination of cholesterol uptake by Caco-2 cells, Rapid Commun. Mass Spectrom. 20 (2006) 3056–3060.

[33] A.E. DeBarber, D. Lutjohann, L. Merkens, R.D. Steiner, Liquid chromatography-tandem mass spectrometry determination of plasma 24S-hydroxycholesterol with chromatographic separation of 25-hydroxycholesterol, Anal. Biochem. 381 (2008) 151–153.

[34] R. Karuna, A. von Eckardstein, K.M. Rentsch, Dopant assisted-atmospheric pressure photoionization (DA-APPI) liquid chromatography–mass spectrometry for the quantification of 27-hydroxycholesterol in plasma, J. Chromatogr. B Analyt. Technol. Biomed. Life Sci. 877 (2009) 261–268.

[35] A. Honda, J. Shoda, N. Tanaka, Y. Matsuzaki, T. Osuga, N. Shigematsu, M. Tohma, H. Miyazaki, Simultaneous assay of the activities of two key enzymes in cholesterol metabolism by gas chromatography–mass spectrometry, J. Chromatogr. 565 (1991) 53–66.

[36] A. Sanghvi, E. Grassi, C. Bartman, R. Lester, M. Galli Kienle, G. Galli, Measurement of cholesterol 7α-hydroxylase activity with selected ion monitoring, J. Lipid Res. 22 (1981) 720–724.

[37] J.M.E. Quirke, C.L. Adams, G.J. Van Berkel, Chemical derivatization for electrospray ionization mass spectrometry. 1. Alkyl halides, alcohols, phenols, thiols, and amines, Anal. Chem. 66 (1994) 1302–1315.

[38] G.J. Van Berkel, J.M. Quirke, R.A. Tigani, A.S. Dilley, T.R. Covey, Derivatization for electrospray ionization mass spectrometry. 3. Electrochemically ionizable derivatives, Anal. Chem. 70 (1998) 1544–1554.

[39] R. Sandhoff, B. Brügger, D. Jeckel, W.D. Lehmann, F.T. Wieland, Determination of cholesterol at the low picomole level by nano-electrospray ionization tandem mass spectrometry, J. Lipid Res. 40 (1999) 126–132.

[40] D.W. Johnson, H.J. ten Brink, C. Jakobs, A rapid screening procedure for cholesterol and dehydrocholesterol by electrospray ionization tandem mass spectrometry, J. Lipid Res. 42 (2001) 1699–1705.

[41] X. Jiang, D.S. Ory, X. Han, Characterization of oxysterols by electrospray ionization tandem mass spectrometry after one-step derivatization with dimethylglycine, Rapid Commun. Mass Spectrom. 21 (2007) 141–152.

[42] A. Honda, K. Yamashita, M. Numazawa, T. Ikegami, M. Doy, Y. Matsuzaki, H. Miyazaki, Highly sensitive quantification of 7α-hydroxy-4-cholesten-3-one in human serum by LC–ESI–MS/MS, J. Lipid Res. 48 (2007) 458–464.

[43] A. Honda, K. Yamashita, H. Miyazaki, M. Shirai, T. Ikegami, G. Xu, M. Numazawa, T. Hara, Y. Matsuzaki, Highly sensitive analysis of sterol profiles in human serum by LC–ESI–MS/MS, J. Lipid Res. 49 (2008) 2063–2073.

[44] A. Honda, K. Yamashita, T. Hara, T. Ikegami, T. Miyazaki, M. Shirai, G. Xu, M. Numazawa, Y. Matsuzaki, Highly sensitive quantification of key regulatory oxysterols in biological samples by LC–ESI–MS/MS, J. Lipid Res. 50 (2009) 350–357.

[45] W.J. Griffiths, S. Liu, G. Alvelius, J. Sjövall, Derivatisation for the characterisation of neutral oxosteroids by electrospray and matrix-assisted laser desorption/ionisation tandem mass spectrometry: the Girard P derivative, Rapid Commun. Mass Spectrom. 17 (2003) 924–935.

[46] W.J. Griffiths, Y. Wang, G. Alvelius, S. Liu, K. Bodin, J. Sjövall, Analysis of oxysterols by electrospray tandem mass spectrometry, J. Am. Soc. Mass Spectrom. 17 (2006) 341–362.

[47] K. Karu, M. Hornshaw, G. Woffendin, K. Bodin, M. Hamberg, G. Alvelius, J. Sjovall, J. Turton, Y. Wang, W.J. Griffiths, Liquid chromatography-mass spectrometry utilizing multi-stage fragmentation for the identification of oxysterols, J. Lipid Res. 48 (2007) 976–987.

[48] K. Hiraoka, I. Kudaka, Negative-mode electrospray-mass spectrometry using nonaqueous solvents, Rapid Commun. Mass Spectrom. 6 (1992) 265–268.

[49] T. Higashi, K. Shimada, Derivatization of neutral steroids to enhance their detection characteristics in liquid chromatography–mass spectrometry, Anal. Bioanal. Chem. 378 (2004) 875–882.

Please cite this article in press as: A. Honda, et al., Highly sensitive and specific analysis of sterol profiles in biological samples by HPLC–ESI–MS/MS, J. Steroid Biochem. Mol. Biol. (2010), doi:10.1016/j.jsbmb.2010.03.030

[50] T. Higashi, N. Takayama, T. Nishio, E. Taniguchi, K. Shimada, Procedure for increasing the detection responses of estrogens in LC–MS based on introduction of a nitrobenzene moiety followed by electron capture atmospheric pressure chemical ionization, Anal. Bioanal. Chem. 386 (2006) 658–665.
[51] G. Singh, A. Gutierrez, K. Xu, I.A. Blair, Liquid chromatography/electron capture atmospheric pressure chemical ionization/mass spectrometry: analysis of pentafluorobenzyl derivatives of biomolecules and drugs in the attomole range, Anal. Chem. 72 (2000) 3007–3013.
[52] M.S. Kuo, J.M. Kalbfleisch, P. Rutherford, D. Gifford-Moore, X.D. Huang, R. Christie, K. Hui, K. Gould, M. Rekhter, Chemical analysis of atherosclerotic plaque cholesterol combined with histology of the same tissue, J. Lipid Res. 49 (2008) 1353–1363.
[53] E.G. Lund, U. Diczfalusy, Quantitation of receptor ligands by mass spectrometry, Methods Enzymol. 364 (2003) 24–37.
[54] W.J. Griffiths, M. Hornshaw, G. Woffendin, S.F. Baker, A. Lockhart, S. Heidelberger, M. Gustafsson, J. Sjövall, Y. Wang, Discovering oxysterols in plasma: a window on the metabolome, J. Proteome Res. 7 (2008) 3602–3612.
[55] K. Yamashita, S. Kobayashi, S. Tsukamoto, M. Numazawa, Synthesis of pyridine-carboxylate derivatives of hydroxysteroids for liquid chromatography–electrospray ionization–mass spectrometry, Steroids 72 (2007) 50–59.
[56] K. Yamashita, M. Okuyama, Y. Watanabe, S. Honma, S. Kobayashi, M. Numazawa, Highly sensitive determination of estrone and estradiol in human serum by liquid chromatography–electrospray ionization tandem mass spectrometry, Steroids 72 (2007) 819–827.
[57] K. Yamashita, M. Takahashi, S. Tsukamoto, M. Numazawa, M. Okuyama, S. Honma, Use of novel picolinoyl derivatization for simultaneous quantification of six corticosteroids by liquid chromatography–electrospray ionization tandem mass spectrometry, J. Chromatogr. A 1173 (2007) 120–128.
[58] K. Yamashita, R. Nakagawa, M. Okuyama, S. Honma, M. Takahashi, M. Numazawa, Simultaneous determination of tetrahydrocortisol, allotetrahydrocortisol and tetrahydrocortisone in human urine by liquid chromatography–electrospray ionization tandem mass spectrometry, Steroids 73 (2008) 727–737.
[59] K. Yamashita, Y. Tadokoro, M. Takahashi, M. Numazawa, Preparation and structural elucidation of the picolinyl ester of aldosterone for liquid chromatography–electrospray ionization tandem mass spectrometry, Chem. Pharm. Bull. 56 (2008) 873–877.
[60] K. Yamashita, M. Okuyama, R. Nakagawa, S. Honma, F. Satoh, R. Morimoto, S. Ito, M. Takahashi, M. Numazawa, Development of sensitive derivatization method for aldosterone in liquid chromatography–electrospray ionization tandem mass spectrometry of corticosteroids, J. Chromatogr. A 1200 (2008) 114–121.
[61] L.L. Smith, Cholesterol Autoxidation, Plenum Press, New York, 1981.
[62] A.K. Batta, G. Salen, S. Shefer, G.S. Tint, M. Batta, Increased plasma bile alcohol glucuronides in patients with cerebrotendinous xanthomatosis: effect of chenodeoxycholic acid, J. Lipid Res. 28 (1987) 1006–1012.
[63] L.J. Meng, W.J. Griffiths, H. Nazer, Y. Yang, J. Sjövall, High levels of (24S)-24-hydroxycholesterol 3-sulfate, 24-glucuronide in the serum and urine of children with severe cholestatic liver disease, J. Lipid Res. 38 (1997) 926–934.
[64] X. Li, W.M. Pandak, S.K. Erickson, Y. Ma, L. Yin, P. Hylemon, S. Ren, Biosynthesis of the regulatory oxysterol, 5-cholesten-3β,25-diol 3-sulfate, in hepatocytes, J. Lipid Res. 48 (2007) 2587–2596.

Please cite this article in press as: A. Honda, et al., Highly sensitive and specific analysis of sterol profiles in biological samples by HPLC–ESI–MS/MS, J. Steroid Biochem. Mol. Biol. (2010), doi:10.1016/j.jsbmb.2010.03.030

Original Paper

Comparison of Biochemical Safety between PEG-IFN α-2a and PEG-IFN α-2b

Yoshiaki Katano[1], Takashi Kumada[2], Isao Nakano[1], Hidenori Toyoda[2]
Masatoshi Ishigami[1], Kazuhiko Hayashi[1], Takashi Honda[1], Hidemi Goto[1]
[1]Department of Gastroenterology, Nagoya University Graduate School of Medicine
65 Tsurumai-cho, Showa-ku, Nagoya 466-8560, Japan. [2]Department of Gastroenterology
Ogaki Municipal Hospital, 4-86 Minaminokawa-cho, Ogaki 503-8502, Japan
Corresponding Author: Yoshiaki Katano, Department of Gastroenterology
Nagoya University Graduate School of Medicine, 65 Turumai-cho, showa-ku, Nagoya 466-8560, Japan
Tel: +81-52-744-2169, Fax: +81-52-744-2178, E-mail: ykatano@med.nagoya-u.ac.jp

ABSTRACT

Background/Aims: Although the efficacy and safety of pegylated-interferon (PEG-IFN) α-2a and PEG-IFN α-2b have been comparatively studied, there are few study results available in which the two PEG-IFN products were strictly compared. To compare the effects of two PEG-IFN products on blood cell profile.

Methodology: The time-course change in blood cell counts was compared between chronic hepatitis C patients with genotype 1b receiving PEG-IFN α-2a/ribavirin and PEG-IFN α-2b/ribavirin combination therapy. The comparison was made after matching patients from the two groups based on ribavirin apparent clearance (CL/F), a surrogate marker of the steady state blood ribavirin level, in order to eliminate the effect of ribavirin. Fifteen pairs of matched patients were selected.

Results: The time-course change in hemoglobin did not differ significantly between the two groups. However, significantly greater reductions in both neutrophil and platelet counts were observed with PEG-IFN α-2a compared to PEG-IFN α-2b. A slightly longer period was required with PEG-IFN α-2a than with PEG-IFN α-2b for a reduction in neutrophil or platelet count large enough to necessitate dose reduction.

Conclusions: Two types of PEG-IFN products affected the blood cell profile in different manners. Long-term monitoring of laboratory test values is necessary with PEG-IFN α-2a.

KEY WORDS: Chronic hepatitis C; Pegylated-interferon; Ribavirin; Blood cell

ABBREVIATIONS: Pegylated-interferon (PEG-IFN); Ribavirin Apparent Clearance (CL/F); Chronic Hepatitis (CHC); Sustained Virological Response (SVR)

INTRODUCTION

The treatment for chronic hepatitis C (CHC) has advanced remarkably in recent years. At present, combination therapy with pegylated-interferon (PEG-IFN) and ribavirin has become the standard therapy worldwide for CHC. Even in patients with refractory CHC characterized by infection with genotype 1 and high viremia levels, complete eradication of the virus in about 50% of all patients has been reported following 48 weeks of this therapy (1-4). In patients with genotype 2/3 virus infection, in whom better response to IFN can be expected, viral eradication has been reported in 90% of all patients receiving this combination therapy (5-8). At present, two preparations of PEG-IFN are available worldwide. PEG-IFN α-2a is IFN α-2a bound to double-stranded 40kD PEG molecule. The molecules in this formulation of PEG-IFN are large in size, resulting in slow absorption, slow disappearance from the blood, and limited distribution in the body. The percentage of elimination of this type of PEG-IFN via the kidneys is also low. PEG-IFN α-2b is IFN α-2b bound to single-stranded PEG. The molecules in this formulation of PEG-IFN are moderate in size (12KD), which allows for extensive distribution in the body. Compared to PEG-IFN α-2a, PEG-IFN α-2b is more easily eliminated via the kidneys, resulting in slightly more rapid disappearance from the blood and less accumulation in the blood. Although the effect of these differences in characteristics between the two formulations of PEG-IFN α on the efficacy, safety, blood levels, and IFN activity has been evaluated in several studies (9-12), no results of direct clinical comparison have yet been reported. A retrospective study was reported on the effect of the differences in characteristics between the two formulations on blood cells (10), but the dosing period was different and there is no assurance of homogeneity of the background variables of the subjects treated with the two formulations. Blood ribavirin levels are also reported to affect hemoglobin concentrations (13-15) and ribavirin is associated with elevation of the platelet count (4-16). Blood ribavirin levels therefore need to be controlled in advance to conduct a comparison of the effects of ribavirin plus PEG-IFN α-2a therapy and ribavirin plus PEG-IFN α-2b therapy on blood cells. By matching the blood ribavirin levels predicted for Week 4 when ribavirin concentrations reach steady state, the time-course change in blood cell counts following treatment with the two PEG-IFN preparations was examined. Virological efficacy of PEG-IFN α-2a plus ribavirin therapy and PEG-IFN

Hepato-Gastroenterology 2009; 56:485-491

TABLE 1 List of Matched Cases

Group	No	CL/F	Sex	Age	Body weight	CCr
PEG-IFN α-2a	A-1	6.954	Female	62	55	72.4
	A-2	8.263	Male	60	57	57.6
	A-3	9.719	Male	66	63	71.9
	A-4	10.320	Female	35	58	89.9
	A-5	10.413	Male	66	60	77.1
	A-6	11.142	Female	53	62.8	107.5
	A-7	11.871	Male	60	67	82.7
	A-8	12.279	Male	45	64	76.8
	A-9	14.536	Male	41	58.2	88.9
	A-10	15.233	Male	51	80	98.9
	A-11	15.455	Male	46	67	97.2
	A-12	17.609	Male	47	69	111.4
	A-13	18.977	Male	24	67	107.9
	A-14	7.718	Female	53	58	74.5
	A-15	16.030	Male	38	75	96.6
PEG-IFN α-2b	B-1	6.076	Female	61	47	62.6
	B-2	8.283	Male	69	58	63.5
	B-3	9.909	Male	64	68	71.8
	B-4	10.381	Female	48	53.5	96.8
	B-5	10.443	Male	64	64.5	75.6
	B-6	11.163	Male	60	70	77.8
	B-7	11.965	Male	46	63.4	75.2
	B-8	12.207	Male	62	56	86.7
	B-9	14.683	Male	53	64	96.7
	B-10	15.370	Male	34	55.6	90.95
	B-11	15.834	Female	42	74	142.7
	B-12	17.084	Male	38	65.4	102.9
	B-13	19.090	Female	31	50.8	158.93
	B-14	8.881	Male	63	65.5	63.7
	B-15	14.219	Male	57	67	96.5

α-2b plus ribavirin therapy was also evaluated although the statistical power to confirm a difference in efficacy was not adequate.

METHODOLOGY

Subjects

The subjects of this study were the patients enrolled into the clinical trials of PEG-IFN α-2a plus ribavirin therapy (Group A: 18 patients) conducted between 2002 and 2004 and PEG-IFN α-2b plus ribavirin therapy (Group B: 25 patients) conducted between 2001 and 2003 at Nagoya University Hospital and Ogaki Municipal Hospital. Only adult patients with CHC had been enrolled. The analysis in the present study was limited to patients infected with genotype 1b virus and with high viral load. Previous history of IFN therapy was not taken into account in patient selection. Patients had to have hemoglobin of ≥12g/dL, neutrophil count of ≥1,500/mm^3, and platelet count of ≥100,000/mm^3. The inclusion criteria are reported in detail elsewhere (4,17). The present study was approved by Institutional Review Board of our center.

TABLE 2 List of Non-Matched Cases

Group	No	CL/F	Sex	Age	Body weight	CCr
PEG-IFN α-2a	A-16	17.796	Male	43	73.5	110
	A-17	19.399	Male	46	84.1	
	A-18	25.408	Male	36	84	151.7
PEG-IFN α-2b	B-16	4.951	Female	65	54	53.1
	B-17	5.259	Female	64	56	55.8
	B-18	5.659	Female	65	48	60.7
	B-19	10.797	Male	64	74.1	78.2
	B-20	12.560	Female	22	44.8	04.015
	B-21	13.002	Male	61	75	91.4
	B-22	13.296	Male	52	64	86.9
	B-23	21.328	Male	32	83.4	125.1
	B-24	27.968	Male	30	85.2	162.7
	B-25	36.170	Male	36	89.7	215.94

Treatment Method

PEG-IFN α-2a (Chugai Pharmaceutical Co., Ltd., Tokyo) was administered once weekly at the dose of 180mg. PEG-IFN α-2b (Schering-Plough K.K., Osaka) was administered once weekly at the dose of 1.5mg/kg. The dose was reduced by half when the criteria for dose reduction became applicable. For both Group A and Group B, ribavirin was administered at the dose of 600mg/day in patients weighing 60kg or less, 800mg/day in patients weighing greater than 60kg but less than 80kg, and 1,000mg/day in patients weighing greater than 80kg. The dose of ribavirin was reduced by 200mg/day when the criteria for dose reduction became applicable. The criteria for the dose reduction of PEG-IFN were: (1) neutrophil count less than 750/mm^3 (for both groups), and (2) platelet count less than 50,000/mm^3 in Group A and less than 80,000/mm^3 in Group B. The criterion for ribavirin dose reduction was a hemoglobin value less than 10g/dL.

Analysis of changes in blood cells

Hematological tests were conducted immediately before, and 1, 2, 3, 4, 8, 12, 16, 20, 24, 28, 32, 36, 40, 44 and 48 weeks after the start of treatment, and also 4, 12 and 24 weeks after the end of treatment. The changes in serum hemoglobin, neutrophil count, and platelet count were analyzed.

Assessment of virological response and blood ribavirin levels

Sustained virological response (SVR) is defined as HCV RNA being undetectable by polymerase chain reaction in serum at 24 week after the end of 48-week treatment. Blood ribavirin concentration at Week 4 was measured in 23 patients by the HPLC method (SRL Inc., Tokyo).

Case matching

The blood level of ribavirin four weeks after the start of treatment was predicted by the method reported by Toyota *et al.* (13). The equation proposed by Kamar *et al.* (18) was used for the calculation of CL/F required for the prediction of the blood level by the Toyota method. Case matching between the two groups was conducted by arranging all 18 patients in

Group A and 25 patients in Group B in the order of CL/F. The pairs of CL/F-matched cases were selected from the two groups on a one-to-one basis based on a CL/F range of less than 2L/hr (equivalent to a predicted blood level of 200ng/mL) as shown in **Table 1**. As a result, 15 matched pairs were identified. **Table 2** shows the background variables of the patients not selected by such matching (3 patients from Group A and 10 patients from Group B).

Statistical analysis

Point estimates of each background variable were expressed as the median, and point estimates of the change in the blood cell counts were expressed as the LS mean. Mann-Whitney's U-test or Fisher's exact test was used for the comparison of the background variables of the 15 selected patients. Analysis of variance (using a general linear mixed effects model) was used for the time-course of changes in the blood cell counts. This analysis was conducted separately to evaluate the effects of treatment and to evaluate recovery after the end of treatment. The hematological parameters at each measurement time point were compared using the *t*-test. $p < 0.05$ (two-sided) was regarded as being statistically significant.

RESULTS

Background variables, dose reduction and discontinuation of treatment

Table 3 shows the background variables of the 15 matched patients from each group (Group A and B). The mean age of the patients in Group B was slightly higher than that in Group A, but there was no significant distribution bias in any background variable between the two groups. Treatment was discontinued in one patient each from each group which was due to the onset of clinical symptoms and not to laboratory test results. The PEG-IFN dose had to be reduced in 5 patients (33%) in Group A and 2 patients (13.3%) in Group B ($p = 0.390$, Fisher's exact test). The cause in all patients was decrease in the neutrophil count. No patient required dose reduction due to decrease in the platelet count. The difference between the two groups in the criteria for dose reduction based on the platelet count therefore did not affect the rate of dose reduction, and there was no necessity to take into account the difference in the dose reduction criteria when comparing the time-course of changes of the platelet count between the two groups. A reduction of the ribavirin dose was required in one patient (6.7%) in Group A and 3 patients (20%) in Group B ($p = 0.598$, Fisher's exact test).

Hemoglobin

Figure 1 shows the time-course of change in serum hemoglobin concentrations with Group A and Group B during and after the end of treatment. With matching for CL/F, the pre-treatment hemoglobin was approximately the same in both groups. During treatment, hemoglobin was slightly lower in Group B than in Group A, and this was thought attributable to the slightly higher percentage of patients weighing less than 60kg and elderly patient in Group B. There was, however, no significant difference between the two groups in the time-course reduction of hemoglobin during treatment (group x time: p= 0.4583, analysis of variance). The greatest reduction in hemoglobin with Group A was 5.5g/dL, and the mean maximum dose reduction rate was 25.1%. With 10 patients, the lowest hemoglobin was observed at Week 40-48. The greatest reduction in hemoglobin with Group B was 6.3g/dL, and the mean maximum dose reduction rate was 28% ($p = 0.237$ *vs.* that in Group A, U-test). No specific trend was observed in the timing of the maximum reduction in hemoglobin, with the lowest level observed at Week 36-48 in 5 patients. No significant difference was also observed between the groups in

TABLE 3 Comparisons of Background Variables

Variable	PEG-IFNα-2a (n=15)	PEG-IFNα-2b (n=15)	*P*
Age (years)	51 [24-66]	57 [31-69]	0.480
Sex (male/female)	11/4	11/4	1.000
Body weight (kg)	63 [55-80]	64 [47-74]	0.520
CCr	88.9 [57.6-111.4]	86.7 [62.6-159]	0.756
CL/F(L/hr)	11.9 [7.0-19.0]	11.7 [6.1-19.1]	0.950
Predicted ribavirin level	2650[1970-2866]	2560[1432-2970]	0.756
Hemoglobin	14.8 [11.6-17.2]	14.5 [12.1-18.2]	0.787
Neutrophil count	2952[1849-5407]	2983[1561-5986]	0.983
Platelet count	17.3 [10.2-25.2]	17.2 [12.6-39.4]	0.740

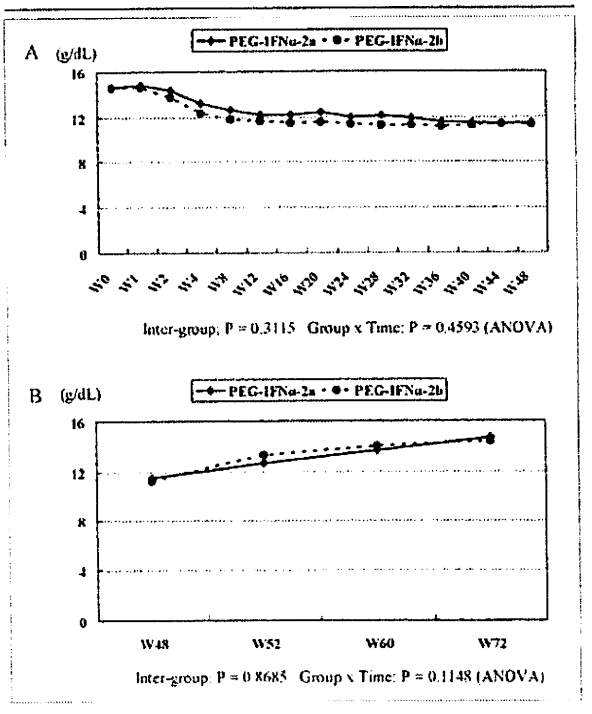

FIGURE 1: Time course of changes in the hemoglobin concentrations during **(A)** and after **(B)** therapy with PEG-IFN α-2a or PEG-IFN α-2b in combination with ribavirin. Data are expressed as LS mean.

recovery in hemoglobin levels after the end of treatment.

Neutrophil count

The neutrophil count before the start of treatment was approximately the same in Group A and Group B (Figure 2). A significant difference, however, was observed in the pattern of change of the neutrophil count during treatment between the two groups (group x time: $P = 0.0185$, analysis of variance). In Group A, a sharp decrease in the neutrophil count was observed from one week after the start of treatment, and it tended to decrease further with time. At all measurement time points during treatment, the neutrophil count was lower in Group A than in Group B. The greatest reduction in neutrophil count was 4,660/mm³ in Group A, and the mean maximum reduction rate was 67.5%. The time point at which the lowest neutrophil count was recorded tended to be later in Group A (after Week 28 in 9 patients) than in Group B. This tendency was particularly marked in patients with a higher body weight. A sharp decrease in the neutrophil count was also observed at one week after the start of treatment in Group B, but the magnitude of the decrease was smaller than in Group A and almost no further decrease was observed subsequently. The maximum reduction of the neutrophil count was 3,205/mm³, and the mean maximum reduction rate was 64.6% ($P = 0.494$ *vs.* that in Group A, U-test). The time point at which the lowest neutrophil count was recorded tended to be earlier (Week 12-24 in 6 patients) than in Group A. The recovery in the neutrophil count after the end of treatment is shown in Figure 2 (B). In Group B, the neutrophil count returned to almost the pre-treatment baseline level by 4 weeks after the end of the treatment while recovery was slower in Group A than in Group B although the difference was not significant.

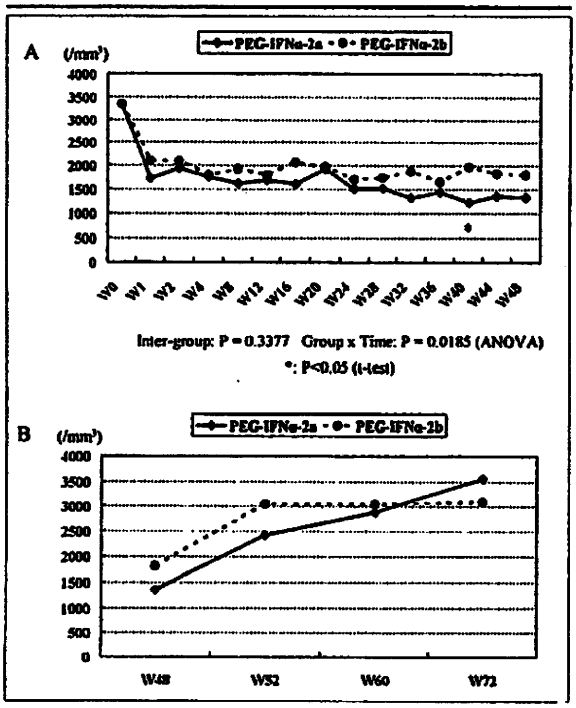

FIGURE 2: Time course of changes in the neutrophil count during (A) and after (B) therapy with PEG-IFN α-2a or PEG-IFN α-2b in combination with ribavirin. Data are expressed as LS mean.

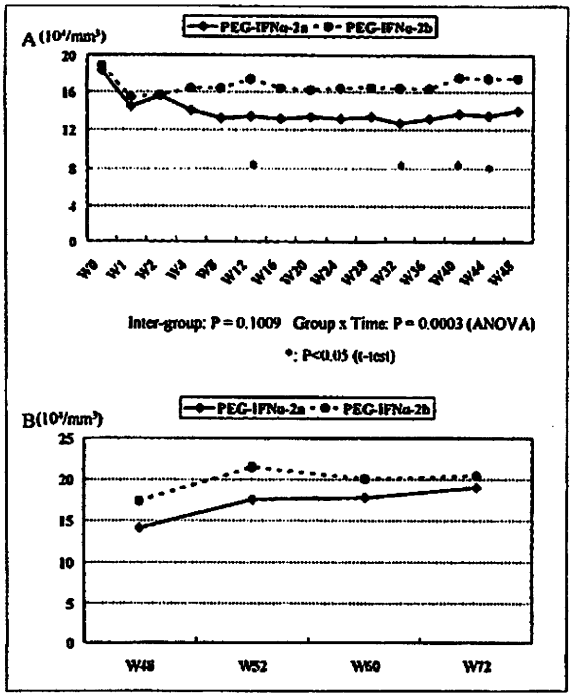

FIGURE 3: Time course of changes in the platelet count during (A) and after (B) therapy with PEG-IFN α-2a or PEG-IFN α-2b in combination with ribavirin. Data are expressed as LS mean.

Platelet count

The pre-treatment platelet count was nearly the same in Group A and Group B. At all measurement time points during the treatment period, however, the platelet count was lower in Group A than in Group B (Figure 3). In Group B in the 4 weeks during which blood ribavirin levels increase to reach steady state, the platelet count was observed to increase and thereafter remained almost unchanged. The greatest reduction in the platelet count was 272,000/mm³ in Group B, and the mean maximum reduction rate was 29.7%. The lowest platelet count was observed within the first 4 weeks in 7 patients and in Week 24-28 in 5 patients. On the other hand, although a slight increase in the platelet count was observed in Week 2 in Group A, decrease was again observed up to Week 8, after which levels remained almost unchanged. The greatest reduction of the platelet count in Group A was 112,000/mm³ and the mean maximum reduction rate was 39.9% ($p = 0.005$ *vs.* that in Group B, U-test). The lowest platelet count was observed at a later time point in Group A compared to Group B, with the lowest platelet count observed within the first 8 weeks in 5 patients and from Week 36 in 4 patients. No patient experienced the rapid reduction of the platelet count in the late stage of treatment. Based on the above results, it was

confirmed that there is a significant difference in the pattern of change in the platelet count between Group A and Group B (group x time: $p = 0.0003$, analysis of variance). As shown in Figure 3(B), the recovery in platelet count after the end of treatment was significantly superior with Group B compared to Group A.

Virological efficacy

SVR was confirmed in 11 out of 15 patients in Group A and in 10 out of 15 patients in Group B. There was no significant difference between the 2 treatment groups (p =1, Fisher's exact test).

DISCUSSION

Fever and changes in the leukocyte count and platelet count are the most frequently encountered reactions to treatment with IFN. Changes in the leukocyte count observed during IFN therapy are due mainly to decrease in the neutrophil count. The decrease in the neutrophil and platelet counts is dependent on the IFN dose level. The maximum decrease in neutrophil count is observed at one week of treatment with PEG-IFN α-2b, followed by maintenance of steady levels. A trend of increase in the platelet count is observed up to 4 weeks of treatment, followed by a slight decrease thereafter and then steady levels until the end of treatment (4). The effect of the IFN dose is also evident from the type of IFN used. In the study conducted by Iino *et al.* using IFN α-2b (4), the decrease in cell counts following the daily administration of 6MIU of IFN α-2b was greater than that seen following the administration of 1.5mg/kg of PEG-IFN α-2b, but when the dose was change to 6MIU administered 3 times a week, the decrease observed was less than with PEG-IFN α-2b. The incidence of patients requiring IFN dose reduction due to decreased neutrophil count was also higher with 1.0μg/kg of PEG-IFN α-2b than with 6MIU of IFN α-2b administered 3 times a week (19). Glue *et al.* (20) reported a dose-dependent reduction of neutrophil and platelet counts following PEG-IFN α-2b monotherapy. Heathcoat *et al.* (21) also reported a dose-dependent reduction of neutrophil and platelet counts following PEG-IFN α-2a monotherapy. It is interesting to note that there was almost no effect on the changes in the neutrophil count by administering the same once-a-week dose in 2 or 3 divided doses (22).

As explained, the efficacy and safety of PEG-IFN α-2b plus ribavirin therapy was first confirmed, followed by PEG-IFN α-2a plus ribavirin therapy. The primary objective of the present study was to compare the safety of PEG-IFN α-2b plus ribavirin therapy to PEG-IFN α-2a plus ribavirin therapy, retrospectively. For this reason, the presence of bias, however unintentional, associated with patient selection cannot be ruled out. When conducting additional post-hoc analysis of data obtained from different studies, it is essential to eliminate potential confounding factors as far as possible. For conducting the comparison of effect on change in blood cells counts between the two PEG-IFN preparations, we therefore matched patients from one group with those from the other group based on the trough level of ribavirin at week 4 of treatment at which time blood ribavirin levels reach steady state (23). Although the ribavirin preparation used differed between the two groups, the amount of ribavirin contained was the same, and the possibility of a difference between the preparations in the drug transfer rate to the blood was ignored. It is known that the magnitude of reduction in hemoglobin associated with ribavirin treatment correlates with blood ribavirin levels (13-15). However, since measurement of blood drug concentrations was not stipulated in the protocols of the clinical trials from which the data were derived for this study, we used CL/F (reported to correlate with the blood ribavirin level at week 4 of treatment at which time blood ribavirin levels reach steady state) (13) as a surrogate indicator. Blood ribavirin levels were measured retrospectively in 23 out of 30 patients, and good correlation ($p<0.05$; Pearson's correlation) between the actual blood ribavirin level and the estimated ribavirin level calculated by CL/F was confirmed. CL/F was therefore considered a good surrogate marker with which to conduct matching. The conditions for matching patients from the two groups are important. According to the reports of Toyota *et al.* and Tsubota *et al.* (13,23), the blood ribavirin level in Japanese patients after 4 weeks of treatment was often in the range of 2,000 to 3,000ng/mL. In the present study, we adopted the lower level (2,000ng/mL) for matching so that the acceptable range could be set as narrow as possible. The width of the possible matching range was set at 200ng/mL based on Tsubota *et al.* (23) who reported that the 95% confidence interval (one-sided) of the blood ribavirin level after the 8 weeks of treatment (at steady state) in the same patients was approximately 200ng/mL. A blood ribavirin level of 200ng/mL is represented by 1.7-4.3(L/hr) on a CL/F basis according to the method reported by Toyota *et al.* (13). To narrow the range as much as possible, we adopted 2L/hr as the criterion for matching. Using this method, 15 pairs of patients were selected from the two groups. Comparison of these patients from Group A (PEG-IFN α-2a) and Group B (PEG-IFN α-2b), expected to have a nearly identical predicted blood ribavirin level, indicated that the changes in hemoglobin was nearly the same. This implies that the effect of ribavirin on changes in the blood cell counts can be ignored in conducting a comparison between Group A and Group B in neutrophil count and platelet count.

The pattern of change of the neutrophil and platelet counts observed in Group B was nearly identical to that in all patients reported with PEG-IFN α-2b plus ribavirin therapy by Iino *et al.* (4). On the other hand, no report of change in the neutrophil count in Japanese patients has yet been published with PEG-IFN α-2a plus ribavirin therapy. In Mexi-

can patients (24), the neutrophil count was reported to be nearly constant after two weeks of treatment. In the present study, however, the neutrophil count in Group A tended to continue to decrease with time, which is slightly different from the pattern reported in Mexican patients. When Group A and Group B in this study were compared, however, the neutrophil count tended to be lower in Group A than in Group B throughout the study period. In particular, Group A showed a tendency towards continued decrease at the later stage of treatment. The platelet count was also lower in Group A than in Group B throughout the treatment period, with the percent decrease being significantly higher in Group A. Group A showed a pattern of significantly lower platelet count as compared to Group B. Schmid *et al.* compared the results of blood cell change in patients receiving 20 weeks of treatment with PEG-IFN α-2a (180mg) plus ribavirin (1,000-1,200mg/day) and those receiving 20 weeks of treatment with PEG-IFN α-2b (1.5mg/kg) plus ribavirin (1,000-1,200mg/day) (10), and reported that although there was no significant difference in the reduction of the hemoglobin or platelet count between the two groups, the reduction in the neutrophil count was significantly greater with PEG-IFN α-2a plus ribavirin. Their results differ slightly from those obtained in our present study, and the discrepancy in the results between the two studies may be associated with the following factors: (1) the mean age of patients was about 7 years older and the mean body weight was about 10kg lower in the present study than in the study conducted by Schmid *et al.* (10), and (2) both the pre-treatment baseline neutrophil count and platelet count in the present study were lower (neutrophil count by about 1,200/mm^3 in the PEG-IFN α-2a group and about 600/mm^3 in the PEG-IFN α-2b group and platelet count about 20,000/mm^3 in both groups) than those in the study reported by Schmid *et al.*. Furthermore, unlike the present study in which the effect of ribavirin on the change in hemoglobin and blood cell counts was eliminated by controlling for the blood ribavirin level (case matching), the study conducted by Schmid *et al.* incorporated no such adjustment. It is noteworthy that when the results of the two studies are compared, the neutrophil count and the platelet count during treatment are similar in both studies despite the differences in the baseline counts. In both studies, the reductions of blood cell counts were more pronounced following treatment with PEG-IFN α-2a although the degree of reductions differed slightly between Japanese and Austrian patients. Better recovery in blood cell counts after the end of treatment was also observed with Group B. Since IFN has a dose-dependent effect on the neutrophil and platelet counts, the better recovery in blood cell counts after the end of treatment in Group B can probably be explained by the difference in the IFN dose level between the two groups (much higher with PEG-IFN α-2a than with PEG-IFN α-2b). The blood PEG-IFN level following a dose of PEG-IFN α-2a was reported to be 15 times higher than that following a dose of PEG-IFN α-2b based on comparison of AUC (11). Interestingly, however, this dose effect on reduction of neutrophil and platelet counts does not affect virological efficacy although the SVR rate with PEG-IFN α-2a plus ribavirin in this study is higher than that in all patients (17).

It is known that the efficacy of PEG-IFN plus ribavirin therapy is associated with the degree of compliance of individual patients with the dosing instructions and that the total dose administered also determines efficacy (4,25). The ultimate goal of the present study was to identify the criteria for the selection of the optimal regimen for individual patients to improve efficacy by increasing the total dose administered. To this end, we evaluated the effects of the two PEG-IFN preparations on the blood cells. Because of the sample size, no significant difference was observed between the two in the incidence of patients requiring treatment discontinuation or dose reduction. However, the magnitude of reduction of the neutrophil count as well as the platelet count was significantly greater with PEG-IFN α-2a than with PEG-IFN α-2b. A reduction of the neutrophil or platelet count large enough to necessitate dose reduction also tended to occur at a later period during treatment with PEG-IFN α-2a. That (1) the IFN dose level was higher in the PEG-IFN α-2a group, (2) PEG-IFN α-2a is administered as a fixed dose of 180mg which may have resulted in a higher relative IFN dose levels in low body weight subjects, and (3) effect on blood cells is observed associated with the higher total dose even in high body weight subjects may account for this. Therefore, when administering PEG-IFN α-2a at the fixed dose of 180mg regardless of body weight, long-term monitoring of laboratory test values for the confirmation of safety is essential.

In conclusion, two types of PEG-IFN products affected the blood cell profile in different manners. It is reasonable to select a treatment regimen that is expected to be safe and effective in individual patients, avoiding the administration of excessive doses.

REFERENCES

1 Manns MP, McHutchison JG, Gordon SC, Rustgi VK, Shiffman M, Reindollar R, Goodman ZD, Koury K, Ling M, Albrecht JK: Peginterferon alfa-2b plus ribavirin compared with interferon plus ribavirin for initial treatment of chronic hepatitis C: a randomised trial. Lancet 2001; 358:958-965.

2 Fried MW, Shiffman ML, Reddy KR, Smith C, Marinos G, Goncales FL Jr, Häussinger D, Diago M, Carosi G, Dhumeaux D, Craxi A, Lin A, Hoffman J, Yu J: Peginterferon alfa-2a plus ribavirin for chronic hepatitis C virus infection. N Engl J Med 2002; 347:975-982.

3 Hadziyannis SJ, Sette H Jr, Morgan TR, Balan V, Diago M, Marcellin P, Ramadori G, Bodenheimer H Jr, Bernstein D, Rizzetto M, Zeuzem S, Pockros PJ, Lin A, Ackrill AM, PEGASYS International Study Group: Peginterferon-alfa 2a and ribavirin combination

therapy in chronic hepatitis C. A randomized study of treatment duration and ribavirin dose. Ann Internal Med 2004; 140:346-355.
4 Iino S, Okita K, Omata M, Kumada H, Hayashi N, Tanikawa K: Efficacy of 48-week combined PEG-interferon α-2b + ribavirin therapy in chronic hepatitis C with genotype I and high virus level – A retrospective comparison with 6-month combined interferon α-2b + ribavirin. Kan Tan Sui (Japanese) 2004; 49:1099-1121.
5 Zeuzem S, Hultcrantz R, Bourliere M, Goeser T, Marcellin P, Sanches-Tapias J, Sarrazin C, Harvey J, Brass C, Albrecht J: Peginterferon alfa-2b plus ribavirin for treatment of chronic hepatitis C in previously untreated patients infected with HCV genotypes 2 or 3. J Hepatology 2004; 40:993-999.
6 Mangia A, Santoro R, Minerva N, Ricci GL, Carretta V, Persico M, Vinelli F, Scotto G, Bacca D, Annese M, Romano M, Zechini F, Sogari F, Spirito F, Andriulli A: Peginterferon alfa-2b and ribavirin for 12 *vs.* 24 weeks in HCV genotype 2 or 3. N Eng J Med 2005; 352:2609-2617.
7 Von Wagner M, Huber M, Berg T, Hinrichsen H, Rasenack J, Heintges T, Bergk A, Bernsmeier C, Häussinger D, Herrmann E, Zeuzem S: Peginterferon-α-2a(40KD) and ribavirin for 16 or 24 weeks in patients with genotype 2 or 3 chronic hepatitis C. Gastroenterology 2005; 129:522-527.
8 Kumada H, Toyota J, Goto K, Imawari M, Fujiwara K, Yokosuka O, Sato N, Yasuda K, Izumi N, Ichida T, Honda M, Kojima K, Yoshioka K, Tomita E, Kumada T, Kato M, Yoshihara H, Shimomura H, Yamada G, Sakisaka S, Tanikawa K: Efficacy of 24-week combined PEG-interferon α-2b + ribavirin therapy in chronic hepatitis C cases with genotype I and low virus level and genotype 2 chronic hepatitis C cases – A comparison with 24-weeek combined interferon α-2b + ribavirin. Kan Tan Sui (Japaneses) 2006; 52:645-663.
9 Meta-analysis Working Group: Efficacy of PEG-IFN alfa-2b *vs.* PEG-IFN alfa-2a+ ribavirin regimens in treatment-naïve chronic HCV patients: a cumulative meta-analysis of retrospective data from 6 clinic sites. Hepatology 2005; 42(Suppl. 1):671A.
10 Schmid M, Kreil A, Jessner W, Homoncik M, Datz C, Gangl A, Ferenci P, Peck-Radosavljevic M: Suppression of haematopoiesis during therapy of chronic hepatitis C with different interferon α mono and combination therapy regimens. Gut 2005; 54:1014-1120.
11 Bruno R, Sacchi P, Maiocchi L, Zocchetti C, Ciappina V, Patruno S, Filice G: Area-under-the-curve for peginterferon alpha-2a and peginterferon alpha-2b is not related to body weight in treatment-naïve patients with chronic hepatitis C. Antiviral Therapy 2005; 10:201-205.
12 Silva M, Poo J, Wagner F, Jackson M, Cutler D, Grace M, Bordens R, Cullen C, Harvey J, Laughlin M: A randomised trial to compare the pharmacokinetic, pharmacodynamic, and antiviral effects of peginterferon alfa-2b and peginterferon alfa-2a in patients with chronic hepatitis C (COMPARE). J Hepatology 2006; 45:204-213.
13 Toyota J, Karino Y, Akaike J, Ohmura T, Sato T, Yamazaki K, Kuwata Y, Iino S: Systemic ribavirin clearance (CL/F) is the factor most closely related to dose reduction and discontinuation of drug therapy for a reason of complication by anemia. Acta Hepatologica Japonica (Japanese) 2005; 46:107-118.
14 Maeda Y, Kiribayashi Y, Moriya T, Maruhashi A, Omoda K, Funakoshi S, Murakami T, Takano M: Dosage adjustment of ribavirin based on renal function in Japanese patients with chronic hepatitis C. Ther Drug Monit 2004; 26:9-15.
15 Donnerer J, Grahovac M, Stelzl E, Kessler HH, Bankuti C, Stadbauer V, Stauber RE: Ribavirin levels and haemoglobin decline in early virological responders and non-responders to hepatitis C virus combination therapy. Pharmacology 2006; 76:136-140.
16 Kowdley KV: Hematologic side effects of interferon and ribavirin therapy. J Clin Gastroenterol 2005; 39(suppl. 1):S3-S8.
17 Kuboki M, Iino S, Okuno T, Omata M, Kiyosawa K, Kumada H, Hayashi N, Sakai T: Peginterferon α-2a (40 KD) plus ribavirin for the treatment of chronic hepatitis C in Japanese patients. J Gastroenterol Hepatol 2007; 22:645-652.
18 Kamar N, Chatelut E, Manolis E, Lafont T, Izopet J, Rostaing L: Ribavirin pharmacokinetics in renal and liver transplantation patients: evidence that it depends on renal function. Am J Kidney Dis 2004; 43:140-146.
19 Bruno S, Cammà C, Di Marco V, Rumi M, Vinci M, Camozzi M, Rebucci C, Di Bona D, Colombo M, Craxi A, Mondelli MU, Pinzello G: Peginterferon alfa-2b plus ribavirin for naïve patients with genotype 1 chronic hepatitis C: a randomized controlled trial. J Hepatology 2004; 41:474-481.
20 Glue P, Fang JW, Rouzier-Panis R, Raffanel C, Sabo R, Gupta SK, Salfi M, Jacobs S: Pegylated interferon-a2b: Pharmacokinetics, pharmacodynamics, safety, and preliminary efficacy data. Hepatitis C Intervention Therapy Group. Clin Pharmacol & Therapy 2000; 68:556-567.
21 Heathcote EJ, Shiffman ML, Cooksley WG, Dusheiko GM, Lee SS, Balart L, Reindollar R, Reddy RK, Wright TL, Lin A, Hoffman J, De Pamphilis J: Peginterferon alfa-2a in patients with chronic hepatitis C and cirrhosis. New Engl J Med 2000; 343:1673-1680.
22 Lurie Y, Rouzier-Panis R, Webster GJ, Dusheiko GM, Laughlin M, Jackson ML, Oren R: Optimal dosing frequency of pegylated interferon alfa-2b monotherapy for chronic hepatitis C virus infection. Clinical Gastroenterol and Hepatol. 2005; 3:610-615.
23 Tsubota A, Hirose Y, Izumi N, Kumada H: Pharmacokinetics of ribavirin in combined interferon alpha-2b and ribavirin therapy for chronic hepatitis C virus infection. Br J Clin Pharmacol 2003; 55:360-367.
24 Juarez-Navarro A, Vera-de-Leon L, Navarro JM, Chirino-Sprung R, Diaz-Hernandez M, Casillas-Davila L, Dehesa-Violante M: Incidence and severity of infections according to the development of neutropenia during combined therapy with pegylated interferon-a2a plus ribavirin in chronic hepatitis C infection. Methods Find Exp Clin Pharmacol 2005; 27:317-322.
25 Davis GL, Wong JB, McHutchison JG, Manns MP, Harvey J, Albrecht J: Early virological response to treatment with peginterferon alfa-2b plus ribavirin in patients with chronic hepatitis C. Hepatology 2003; 38:645-652.

B-Mode Ultrasound With Algorithm Based on Statistical Analysis of Signals: Evaluation of Liver Fibrosis in Patients With Chronic Hepatitis C

Hidenori Toyoda[1]
Takashi Kumada[1]
Naohisa Kamiyama[2]
Katsuya Shiraki[3]
Kojiro Takase[4]
Tadashi Yamaguchi[5]
Hiroyuki Hachiya[6]

OBJECTIVE. The purpose of this study was to evaluate the degree of liver fibrosis in patients with chronic hepatitis C by use of a method in which the homogeneity of the tissue texture of the liver on B-mode ultrasound images is analyzed on the basis of results of a statistical chi-square test of the echo amplitudes. The method includes an algorithm for removing small structures, such as cross sections of the thin vessels, in the background texture to minimize differences in analysis results between users.

SUBJECTS AND METHODS. Analysis was performed on images of 148 patients with histologically proven chronic hepatitis C without cirrhosis. The peak value of the C_m^2 (modified chi-square distribution) histogram was calculated from B-mode ultrasound images, and the resulting value was compared with the histologic fibrosis grade.

RESULTS. The peak C_m^2 histogram value for grade F3 fibrosis was higher than that for grades F0 and F1 ($p < 0.0001$) and F2 ($p = 0.0003$). The value for grade F2 was higher than that for grades F0 and F1 ($p = 0.0027$). The values gradually increased with an increase in liver fibrosis grade, although no difference was found between grades F0 and F1.

CONCLUSION. The grades of liver fibrosis in patients with chronic hepatitis C are well discriminated with the B-mode ultrasound–based analysis algorithm without discrimination between grades F0 and F1. Findings on conventional ultrasound images may reflect progression of liver fibrosis even in the absence of cirrhosis.

Keywords: algorithm, B-mode ultrasound, chronic hepatitis C, liver fibrosis

DOI:10.2214/AJR.07.4047

Received March 31, 2008; accepted after revision February 5, 2009.

The employment status of N. Kamiyama at Toshiba Medical Systems did not influence the data in this study.

[1]Department of Gastroenterology, Ogaki Municipal Hospital, 4-86 Minaminokawa, Ogaki, Gifu 503-8502, Japan. Address correspondence to T. Kumada (tkumada@he.mirai.ne.jp).

[2]Ultrasound Division, Toshiba Medical Systems Corporation, Otawara, Japan.

[3]Department of Gastroenterology, Mie University School of Medicine, Tsu, Japan.

[4]Department of Medicine, Shutaikai Hospital, Yokkaichi, Japan.

[5]Research Center for Frontier Medical Engineering, Chiba University, Chiba, Japan.

[6]Department of Mechanical and Control Engineering, Tokyo Institute of Technology, Tokyo, Japan.

AJR 2009; 193:1037–1043

0361–803X/09/1934–1037

B-mode ultrasound imaging is highly sensitive to changes in the acoustic properties of tissues, and abnormalities are often diagnosed on the basis of recognition not only of the shapes and motion of important structures but also of subtle changes in tissue texture. It is well known that B-mode images include granular patterns known as speckle and that speckle is not directly related to the scattering structures in tissues but is the result of coherent accumulation of random scattering from within the resolution cell [1–3]. It is also known that the probability density function (PDF) of the echo amplitude from many sources of random scatter is characterized by the Rayleigh distribution [1, 2]. Because normal liver parenchyma is mainly composed of a 3D arrangement of many structures smaller than the wavelength of the typical ultrasound pulse used in clinical examinations, the statistics of the echo amplitudes in a normal liver fit the Rayleigh PDF [3]. The PDF of the echoes does not, however, fit the Rayleigh PDF in livers that contain fibrosis, including cirrhotic livers, because the nodules and fibrous structures that develop are larger than the ultrasound wavelength. In severe liver fibrosis such as cirrhosis, these nodules and fibrous structures in the liver can be seen on B-mode images. It is difficult, however, to differentiate such small structures from speckle in patients with mild cirrhosis or in patients with fibrosis but not cirrhosis. In routine clinical practice, an objective and quantitative method of evaluating liver fibrosis on B-mode images would be useful for follow-up of patients with chronic liver disease.

Several studies have addressed the issue of quantitative ultrasound examination of hepatic fibrosis by use of statistical data on the ultrasound echo signals [4, 5], texture analysis of B-mode images [6, 7], assessment of scattering properties [8, 9] and fractal dimensions of the scattering signals [10], and evaluation of other considerations of PDFs more suitable for liver tissue [11]. We [12–14] have reported results on the tissue characterization of cirrhotic livers with radiofrequency echo signals. We sampled radiofrequency signals in more

than 100 patients, including some with normal livers, and compared them with the pathologic fibrosis grade determined at examination of biopsy specimens. We found that differences between normal and cirrhotic livers could be detected by analysis of root mean square error between the Rayleigh PDF and the statistical results [12], the constant false alarm rate [13], and the fibrosis extraction ratio [14], which reflects the amount of fibrous tissue in the liver extracted with our proposed signal processing. Our method makes it possible to clearly recognize structures in the liver in three dimensions, but the presence of structures such as fine vessels impedes high-speed processing. In addition, radiofrequency signals should be sampled with great care in research-based statistical analysis to avoid including unnecessary structures such as vessel walls and the diaphragm. Therefore, a large amount of time is needed to sample radiofrequency signals for detailed analysis, making this method unsuitable for routine examinations.

A clinically useful and reliable evaluation method of echo signals for routine examinations requires both simplicity and robustness in addition to accuracy. The results of the analysis should not be affected by slight differences in the way measurement is performed. We present a theoretic description of the proposed method, which is based on the statistical chi-square test and includes an algorithm for removing small structures such as cross sections of the thin vessels from the background texture to minimize variation in the analysis results obtained by different users. We analyzed the amplitudes of the echo data of 148 patients with histologically proven chronic hepatitis C without cirrhosis and evaluated the results by comparing them with the histologic fibrosis grades determined at biopsy.

Subjects and Methods

Principle of Analysis

The algorithm described was based on findings of previous studies [12, 13], which showed that the PDF of the echo signals can be approximated by the Rayleigh distribution in normal liver but cannot be approximated if there is an increase in fibrosis. The proposed algorithm includes a procedure for differentiating fibrotic changes and small vessels to achieve both operational simplicity for the user and robustness of the measurement results.

The equation for Rayleigh distribution is as follows:

$$p(x) = \frac{2x}{\sigma^2} e^{-(x^2/\sigma^2)} \quad (1)$$

where σ is a scale parameter indicating the variance of the echo envelope. Because σ has various values according to the intensity of the echo signal x, on B-mode images $p(x)$ does not always have the same value that the speckle generated. The chi-square test is the most well-known method for determining whether a difference exists between the sample variance σ^2 and the population variance σ_0^2. The sample variance σ^2 is calculated as follows:

$$\sigma^2 = \frac{1}{n-1}\sum_{i=1}^{n}(x_i - \mu)^2 \quad (2)$$

where x_i is a value in the sample, μ is the average of the samples, and n is the number of samples. With the sample variance, the χ^2 calculated in equation 3 has a chi-square distribution with $n - 1$ degrees of freedom:

$$\chi^2 = (n-1)\frac{\sigma^2}{\sigma_0^2} \quad (3)$$

The chi-square test is performed under the null hypothesis of $\sigma^2 = \sigma_0^2$ to determine whether the hypothesis can be rejected. We use the adjusted chi-square distribution [14] defined by the following similar formula:

$$C^2 = \frac{\sigma^2}{\sigma_0^2} \quad (4)$$

The adjusted chi-square distribution is defined as $C^2 = \chi^2 / (n - 1)$. The limit value $x \to \infty$ of the chi-square distribution (equation 2) changes according to the number of samples (degrees of freedom), whereas the limit of the adjusted chi-square distribution is always 1 irrespective of the degrees of freedom.

Problems arise in attempts to apply this general model to analysis of liver disease whether or not the echo signals are statistically normal. First, in general statistical testing, a set of samples is assumed to have an approximately normal distribution, and the echo amplitudes have a Rayleigh distribution. This problem can be avoided if a large number of samples are used, because the Rayleigh distribution itself has two independent normal variables. Second, population variance is required but corresponds to the variance for normal liver. It can be difficult to obtain the true value in a chronically diseased liver, and it does not make sense to use the value from the normal liver of another patient because the variance changes owing to the attenuation of liver tissue, the settings of the diagnostic ultrasound equipment such as gain, and the amount of subcutaneous fat. As does $p(x)$ in equation 1, variance has various values even in normal livers. To address this problem, we propose a method for determining an approximate σ_0^2 value from the average of the samples described in step 1. The method for obtaining the proposed parameter, defined as the C_m^2 histogram, consists of the three following steps.

Step 1: Introduction of the Approximate σ_0^2

If samples are well approximated in the Rayleigh distribution, the relation between the average μ and the variant σ_R^2 is as follows:

$$\sigma_R^2(\mu) = \left(\frac{1}{\pi} - 1\right)\mu^2 \quad (5)$$

In this case, the variance calculated theoretically from the average is more robust, that is, the value of the average does not change substantially if a discrete structure such as a cross section of a nearby vessel is included in the samples. The modified average μ_m is described as follows:

$$\mu_m = \frac{1}{N_m}\sum x_i \,(x_i < \mu + \alpha\sigma) \quad (6)$$

where x_i is a sample extracted from all samples so that $x_i < \mu + \alpha\sigma$ (where α is a coefficient that we call the removal threshold) and N_m is the number of extracted samples. In a combination of equations 5 and 6, the approximate σ_0^2 is defined as follows:

$$\sigma_0^2 \Rightarrow \sigma_R^2(\mu_m) = \left(\frac{4}{\pi} - 1\right)\mu_m^2 \quad (7)$$

Step 2: Introduction of the Modified Adjusted Chi-Square Distribution C_m^2

In a manner similar to that in equation 6, the modified variance is defined as follows:

$$\sigma_m^2 = \frac{1}{N_m - 1}\sum (x_i - \mu)^2 \,(x_i < \mu + \alpha\sigma) \quad (8)$$

where x_i is a sample extracted from all samples as $x_i < \mu + \alpha\sigma$ (where α is the removal threshold) and N_m is the number of extracted samples. The aim of obtaining σ_m^2 is to achieve robustness from the locally included discrete structures. Using σ_m^2 we define the modified adjusted chi-square distribution as follows:

$$C_m^2 = \frac{\sigma_m^2}{\sigma_R^2(\mu_m)} = \left(\frac{\pi}{4-\pi}\right)\frac{\sigma_m^2}{\mu_m^2} \quad (9)$$

Using equation 9, we perform a statistical test whether or not the null hypothesis $\sigma^2 = \sigma_0^2$ is rejected. Furthermore, C_m^2 is related as follows to the signal-to-noise ratio (SNR) as defined previously [1] except for the $x_i < \mu + \alpha\sigma$ extraction procedure:

$$C_m^2 \cong \left(\frac{\pi}{4-\pi}\right)\frac{1}{SNR^2} \quad (10)$$

If the samples have a Rayleigh PDF, C_m^2 approaches 1 as the SNR approaches

$$\sqrt{\pi / (4 - \pi)} \cong 1.91.$$

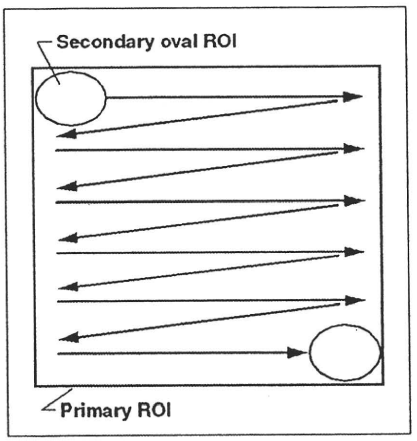

Fig. 1—Schematic shows primary and secondary regions of interest (ROI) for analysis.

Step 3: Introduction of the C_m^2 Histogram

The proposed algorithm has two levels of regions of interest (ROIs) (Fig. 1). The user manually sets the primary ROI in the liver tissue to avoid large vessels, the area in which the acoustic wave is not clearly irradiated, and the area in which multiple reflection is confirmed. The secondary ROI, which is smaller than the primary ROI, automatically sweeps within the primary ROI. The minimum size of the secondary ROI is equivalent to the resolution of the ultrasound beam irradiated in the liver. In general, the size of the secondary ROI is set to more than double the size of the resolution so that a sufficient number of samples can be acquired to maintain the precision of the statistical analysis. The primary ROI contains a large number of secondary ROIs. The results for C_m^2 in the samples in the secondary ROI are calculated multiple times owing to the sweeping steps. All results for C_m^2, which is a ratio of a theoretic calculated value and an actual measurement value, are plotted on a histogram (Fig. 2). If the primary ROI includes mostly the speckle pattern, the C_m^2 histogram shows a peak of 1.0 with a small SD (curve a, Fig. 2). If the primary ROI includes chronic fibrosis, the C_m^2 histogram can be expected to change to curve b, which has a broader peak and a larger SD. Because large structures, such as the walls of large veins and the diaphragm, cannot be removed with this algorithm, the primary ROI is drawn by the user to avoid large structures that can be easily differentiated. Even though the primary ROI may inadvertently be drawn to include the edges of such structures to a slight degree, large values of C_m^2 appear as minor components in the histogram, shown as NS in Figure 2.

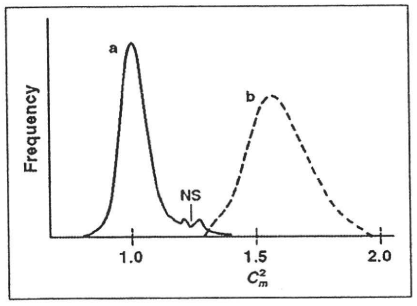

Fig. 2—C_m^2 histogram. Curve a, which has peak of 1.0 and small SD, indicates primary region of interest includes mostly speckle pattern. Curve b, which has broader peak and larger SD than curve a, indicates primary region of interest includes chronic fibrosis. NS indicates minor component.

Equipment Used for Data Acquisition

The amplitudes of the echo signals received in each B-mode scan line were obtained with a prototype system based on a commercially available diagnostic ultrasound system (SSA-770A, Toshiba Medical Systems) with a convex transducer (6.0-MHz center frequency, PVM-674BT, Toshiba Medical Systems). The transmission and reception frequencies of the ultrasound system were 3.5 MHz and 7.0 MHz (harmonic mode) with a 40-MHz sampling frequency. The amplitude data used for analysis were antilogged linear data calculated from 15-bit logged data. The scan-line density and amplitude data in each scan line (15-bit linear) were 380 lines/90° and 100 samples/mm.

For analysis of the C_m^2 histogram, we developed a PC-based program written in C++. The user drew the primary ROIs on the reconstructed B-mode image after scan conversion, and the analysis was performed with the linear amplitude data before scan conversion corresponding to the ROI on the B-mode image. The user can draw multiple primary ROIs on one image so that large structures are not included in the ROIs. The secondary ROI, which is automatically preset on the basis of ultrasound transmission–reception conditions, sweeps all of the primary ROIs, and the results are classified step by step. The C_m^2 histogram is finally obtained with all of the results for the multiple ROIs. For simplicity, the displayed C_m^2 histogram value is calculated to two decimal places and multiplied by 100 (e.g., 1.2345 = 123).

Preliminary Experiments

To validate the modified variance σ_m^2 and to determine the removal threshold α, we conducted preliminary experiments using echo data obtained from an agar phantom and normal and cirrhotic livers. A tissue-equivalent agar phantom (RMI 403GS, Gammex) was used as the target object. This phantom had an attenuation coefficient of 0.5 dB/MHz/cm, the same as the standard attenuation of normal liver tissue, and included thin wires and cysts mimicking high scatter relative to the background.

Validation in Patients With Chronic Hepatitis C With Various Degrees of Fibrosis

One hundred forty-eight patients with chronic hepatitis C who underwent liver biopsy were consecutively enrolled in this study between May 2003 and December 2004. The diagnosis of chronic hepatitis C was based on detection of hepatitis C virus RNA with the nested reverse transcription–polymerase chain reaction method and histologic confirmation of chronic hepatitis at liver biopsy. Informed consent was obtained from each patient enrolled in the study, and the study design was in conformity with the ethical guidelines of the Declaration of Helsinki as reflected in a priori approval by the human research committee at our institution. Table 1 summarizes the characteristics of the patients. The study group included 63 men and 85 women with a median age of 60 years (range, 20–74 years).

Liver biopsy specimens were obtained percutaneously with a 16-gauge needle. Needle biopsy was performed in the S8 segment of the right lobe of the liver, where no large vessels exist, to avoid intraperitoneal bleeding due to the needle biopsy. The specimen was fixed in 10% formalin and stained with H and E, Masson's trichrome, silver impregnation, and periodic acid–Schiff after diastase digestion.

The degree of fibrosis in the liver biopsy specimens obtained from the 148 patients was determined according to the following criteria [15] with fibrosis graded on a scale of F0 to F4: F0, no fibrosis; F1, mild fibrosis, fibrous portal expansion; F2, moderate fibrosis; F3, severe fibrosis, bridging fibrosis (portal–portal or portal–central linkage); and F4, cirrhosis. None of the patients in the study was judged to have F4 fibrosis. The degree of hepatic steatosis was classified into four groups, as follows: none (absent), mild (< 10%), moderate (10–30%), or severe (> 30%). None of the patients was judged to have severe steatosis. The histologic findings for each specimen were interpreted by two pathologists working independently. If there was a discrepancy between the interpreters' diagnoses, more than two other interpreters reevaluated and discussed the case until consensus was reached.

B-mode images and radiofrequency-based echo data were acquired and stored on the day of liver biopsy with an approximately 4-hour interval after biopsy in a routine ultrasound examination. Patients had undergone liver biopsy without drinking and eating for more than 6 hours, and the fasting continued in the interval between liver biopsy and the ultrasound examination. Acquisition of the data for analysis was performed at the area

TABLE 1: Characteristics of Study Patients (n = 148)

Characteristic	Value
Sex	
Men	63
Women	85
Age (y)	60 (20–74)
Fibrosis grade	
F0	14
F1	66
F2	47
F3	21
Hepatic steatosis	
None	115
Mild	26
Moderate	7
Body mass index	22.6 (16.8–32.0)
Viral concentration (KIU/mL)	1,200 (11–6,600)
Hepatitis C virus genotype	
1	90
2	58
Platelet count ($\times 10^4$/mm^2)	16.8 (7.3–31.8)
Aspartate aminotransferase concentration (IU/L)	35 (14–221)
Alanine aminotransferase concentration (IU/L)	42 (10–669)
γ-glutamyl transpeptidase concentration (IU/L)	30 (8–506)
Total bilirubin concentration (mg/dL)	0.6 (0.2–1.6)
Hyaluronic acid concentration (ng/mL)	68 (9.0–1,540)

Note—Continuous values are expressed as median with range in parentheses. Other values are numbers of patients.

biopsied. The quantification software, which was based on the statistical chi-square test, was validated for the echo data corresponding to the liver parenchyma, and the value was calculated for each patient. The focal point was set in the range of 4–6 cm according to the size of the liver. The shape of the secondary ROI was determined in 23 × 60 samples (1,013 samples in total) so that the shape was as close to circular as possible and the number of samples was 1,000. The increment value of the sweeping secondary ROI was five samples. To evaluate the reliability of the analysis, we paid close attention to the peak (statistical mode) of the C_m^2 histogram.

Statistical Analysis

The data were expressed as median and range. Comparisons were performed with the Mann-Whitney U test. All p values were two-tailed, and $p < 0.05$ was considered statistically significant. Statistical analysis was performed with JMP software (version 5.0, SAS Institute).

Results

Preliminary Experiments

The results of basic examinations of models of normal and diseased livers in the agar phantom are shown in Figures 3A–3C. The figures are magnified B-mode images of a homogeneous region, a homogeneous region containing a cross section of wire simulating the wall of a minute portal vein in a normal liver to show echo signals that interfere with speckle, and an inhomogeneous region that imitates thick fibrous tissue intermingling with normal liver. Figure 4 shows the statistical results for σ^2 and σ_R^2 as described in equations 2 and 5 for an oval secondary ROI measuring 23 × 60 samples (1,013 samples in total) swept from left to right in the regions in Figure 3. With regard to the results in the homogeneous region (Fig. 4A), σ_R^2 is flat, similar to σ^2, indicating that the samples are closely approximated by the Rayleigh PDF. In the results for Figure 4B, σ^2 is markedly affected by the strong scatter, but σ_R^2 is less affected because averaging reduces the discrete high-echo signals. In Figure 4C, the variation in σ_R^2 is relatively large because the non-Rayleigh distribution affects the average. From these results, it can be seen that σ_R^2 is robust against locally included small structures.

For calculation of μ_m and σ_m^2, the optimal value of the removal threshold α should be determined. We placed the secondary ROIs in a homogeneous region, an inhomogeneous region, and a homogeneous region containing the cross section of a vessel. Figure 5 shows the modified adjusted chi-square C_m^2 with various α values. With regard to the results in the homogeneous agar phantom (Fig. 3A; curve a, Fig. 5), the value of C_m^2 did not change for $\alpha \geq 5$, indicating that there are few exceptional samples of $\alpha \geq 5$ that affect the C_m^2 value. Similarly, in the calculated results (curve b), C_m^2 did not change for $\alpha \geq 7$ in the region containing the cross section of a vessel shown in Figure 3B. However, in the calculated results for inhomogeneous liver (Fig. 3C; curve c, Fig. 5) C_m^2 changes because of the various α values. This effect was the same at calculated results of C_m^2 in another heterogeneous medium (curve d, Fig. 5). On the basis of these results, we set α to 7 to remove local structures without a large influence on the Rayleigh PDF.

Validation for Patients with Chronic Hepatitis C

Examples of C_m^2 histograms are shown in Figure 6. The peak of the C_m^2 histogram for the agar phantom (Fig. 6A) was approximately 100 with a smaller variant. The typical C_m^2 histogram pattern for grade F1 fibrosis (Fig. 6B) had a slightly higher peak value than that of the homogeneous agar phantom, and it made the shape of the curve asymmetric. We believe these results were influenced by minute fibrous tissue generated in the Glisson capsules or by small portal venous walls because these tendencies can be confirmed in the different values of curves a and b in Figure 5. With regard to the results for grades F2 (Fig. 6C) and F3 (Fig. 6D) fibrosis, both the peak and the variant were large owing to the more advanced grades of fibrosis.

The median values for peak C_m^2 histograms according to stage of chronic hepatitis are shown in Figure 7. The values were 124.5 (range, 109.5–148.0) for patients with fibrosis grade F0 or F1, 131.5 (range, 116.0–146.0) for patients with fibrosis grade F2, and 144.0 (range, 117.5–154.0) for patients

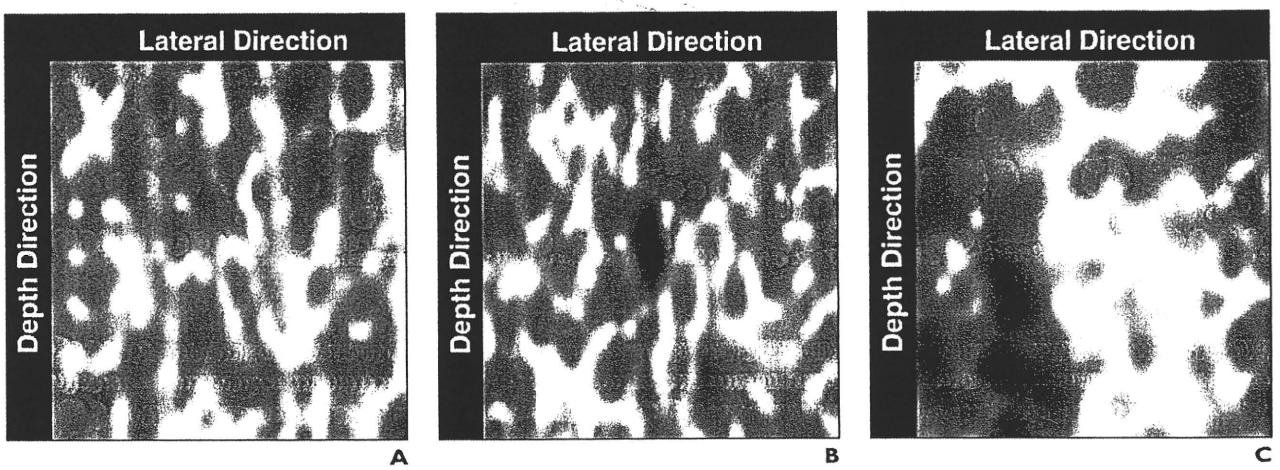

Fig. 3—Magnified B-mode ultrasound images of agar phantom.
A, Homogeneous region.
B, Region containing wire cross section.
C, Inhomogeneous region.

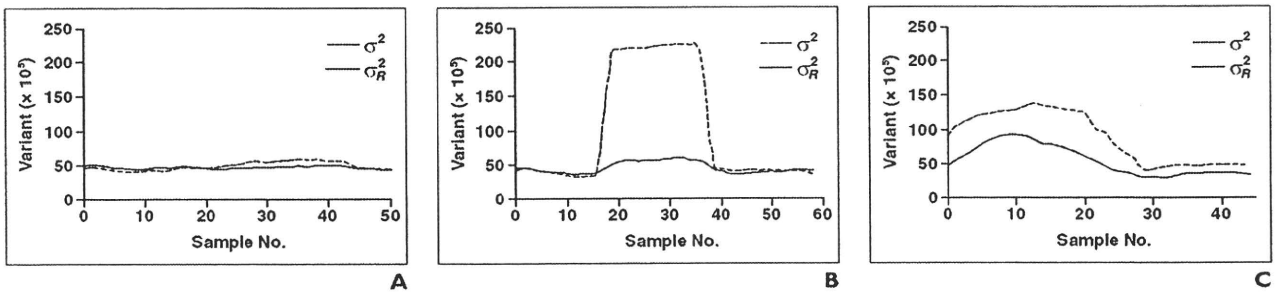

Fig. 4—Statistical results for two variances.
A, Graph shows results for homogeneous region corresponding to Figure 3A.
B, Graph shows results for region containing wire cross section corresponding to Figure 3B.
C, Graph shows results for inhomogeneous region corresponding to Figure 3C.

with fibrosis grade F3. The peak C_m^2 histogram value for F3 was higher than that for F0 or F1 ($p < 0.0001$) and F2 ($p = 0.0003$), and the value for F2 was higher than that for F0 or F1 ($p = 0.0027$). A significant increase in the median peak C_m^2 histogram value was observed in association with progression of fibrosis grade. However, no statistically significant increase in the median peak C_m^2 histogram value was observed between patients with grade F0 fibrosis and those with F1 fibrosis (data not shown). In these analyses, α was fixed at 7, which is the value calculated under almost ideal conditions, because for many of the F0 data, the relation between α and C_m^2 in a homogeneous speckle converged to the steady value similar to that of curves a and b in Figure 5.

Discussion

Evaluation of liver fibrosis is important in the management of patients with chronic hepatitis C. Histologic evaluation of specimens obtained at liver biopsy is the only reliable and accepted method of evaluation of hepatic fibrosis. However, biopsy is invasive and carries the risk of intraperitoneal bleeding. Several methods of elastography of liver stiffness that are based on ultrasound shear waves have been described [16–20], and some of the methods are in use for noninvasive assessment of liver fibrosis [16, 19, 21]. Although they can be used to evaluate the average stiffness of the liver in a single measurement with special

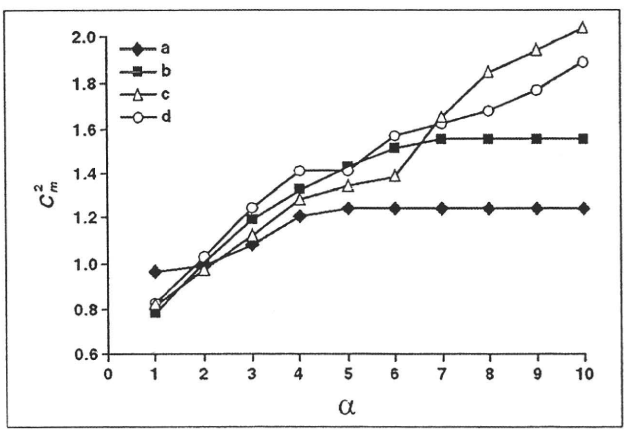

Fig. 5—Graph shows modified adjusted chi-square C_m^2 with various α values. Curves a–c correspond to data in Figures 4A–4C. Curve d shows calculated results in another inhomogeneous region.

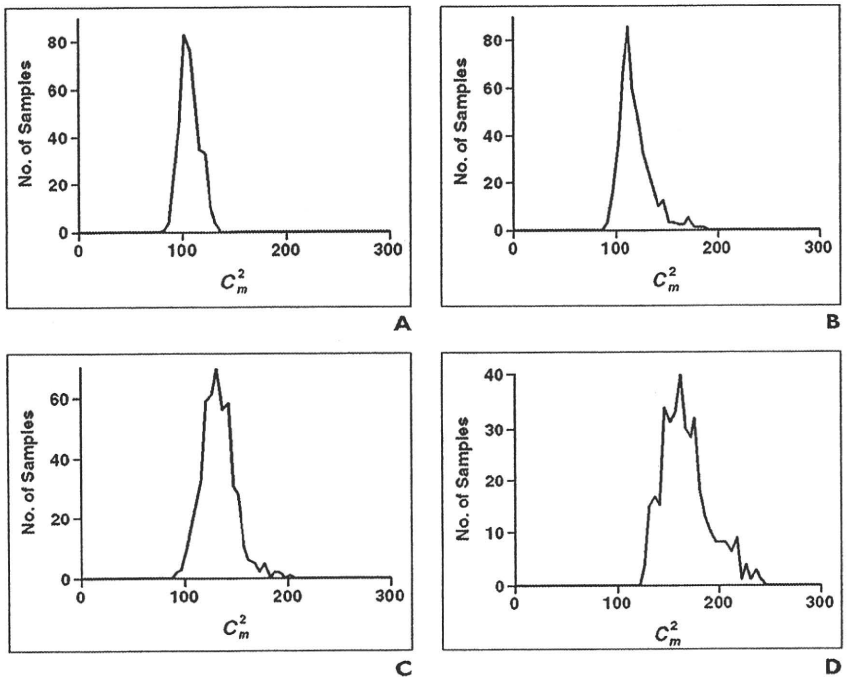

Fig. 6—Examples of C_m^2 histograms.
A, Agar phantom.
B, Liver with grade F1 fibrosis.
C, Liver with grade F2 fibrosis.
D, Liver with grade F3 fibrosis.

equipment, these methods do not yield estimates of local tissue properties or information about the heterogeneity of the liver structure. In contrast, the feature of our proposed method is assessment of the echo signals from multiple local tissues.

B-mode images of the liver include a granular pattern known as speckle. Sonographers know that speckle changes from homogeneous to heterogeneous with the progression of liver fibrosis toward cirrhosis. This finding has been subjective, however, and has not been analyzed objectively. The results of our study show that the peak value of a C_m^2 histogram may be associated with an increase in the grade of liver fibrosis, making it possible to evaluate the degree of liver fibrosis by analysis of B-mode images. We believe that our method may be an ultrasound tool for noninvasive evaluation of liver fibrosis, making it possible to easily evaluate liver fibrosis during routine B-mode ultrasound examinations.

We focused on the peak value of the C_m^2 histogram as an index of liver fibrosis on B-mode images because other values, such as the average or SD of the C_m^2 histogram, are strongly affected by small vessels locally present even in normal livers. Because of the use of the peak value (mode), the shape of the histogram was not included in the analysis. For example, the shapes of the histograms for the agar phantom (Fig. 6A) and for fibrosis grade F0 (normal liver, not shown) were markedly different, which would indicate features such as the presence of vessels (wall and blood flow) and the heterogeneity of Glisson capsules in the human liver, whereas the peak C_m^2 histogram values were similar. This finding suggests that the peak value has limitations and cannot fully represent the characteristics of liver texture. Multiple parameters are needed for more comprehensive characterization.

Although differences in the median value of the peak C_m^2 histogram were observed between different fibrosis grades, there was overlap between adjacent grades. In particular, some F0 and F1 cases had large C_m^2 values. When we reviewed the B-mode images in these cases, cross sections of vessels were sometimes visualized on the images. This finding suggests that users should obtain scan images with special care to exclude such structures from the images being analyzed. The evaluation of fibrosis, therefore, depends on the choice of ROI, which should be improved in the future. Side-lobe artifacts and ultrasound attenuation also can affect the results. Improvement in the SNR should reduce such exceptions.

Conversely, the pathologic results on fibrosis in liver biopsy specimens do not always accurately represent the fibrosis grade of the entire liver. This fact may be another cause of the discrepancies observed in liver fibrosis between the peak C_m^2 histogram value and the pathologic results. Although liver biopsy is the reference standard in assessment of liver fibrosis, biopsy samples usually are small, causing bias in the histologic diagnosis of liver fibrosis. As a result, pathologic results sometimes differ, even in the same patient, depending on the site of the liver biopsy and the pathologist performing the

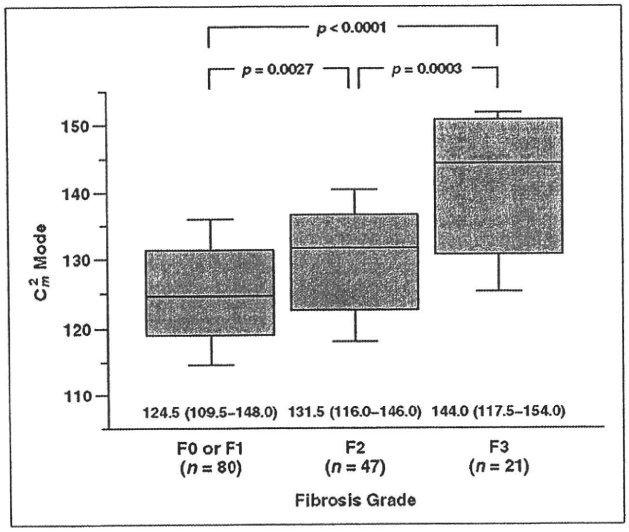

Fig. 7—Graph shows median values with range in parentheses for peak C_m^2 histogram according to stage of chronic hepatitis.

evaluation. Improvement in the evaluation of liver fibrosis on B-mode images should overcome these biases in the future.

We have proposed a method for analyzing C_m^2 histograms of liver tissue that entails analysis of the statistical characteristics of the echo signals. Our findings indicate that results with this B-mode-based algorithm correlate well with fibrosis grade in patients with chronic hepatitis C, even when the focus is on patients without cirrhosis. Although exceptions were found in the analysis results, in general the results closely reflect the homogeneity of the liver texture as visualized on B-mode images. However, significant overlap between fibrosis grades was found in the data in the B-mode-based analysis. Additional studies are needed for more sensitive and accurate evaluation of fibrosis grade on B-mode images of the liver. Analysis of multiple parameters, including the variant, average, and symmetry of the shape of the C_m^2 histogram as well as the peak C_m^2 histogram value, is expected to improve sensitivity and accuracy. An algorithm for automatic removal of groups of small vessels also should lead to further improvement. In addition, application of this method to other diffuse liver diseases, including chronic hepatitis B and nonalcoholic fatty liver disease, should be investigated.

References

1. Burckhardt CB. Speckle in ultrasound B-mode scans. *IEEE Trans Sonics Ultrason* 1978; 25:1–6
2. Wagner RF, Smith SW, Sandrik JM, Lopez H. Statistics of speckle in ultrasound B-scans. *IEEE Trans Sonics Ultrason* 1983; 30:156–163
3. Tuthill TA, Sperry RH, Parker KJ. Deviations from Rayleigh statistics in ultrasonic speckles. *Ultrason Imaging* 1988; 10:81–89
4. Mohana Shankar P. A general statistical model for ultrasonic backscattering from tissue. *IEEE Trans Ultrason Ferroelectr Freq Control* 2000; 47:727–736
5. Fujii Y, Taniguchi N, Wang Y. Clinical application of a new method that segments the region of interest into multiple layers for RF amplitude histogram analysis in the cirrhotic liver [in Japanese]. *J Med Ultrason* 2001; 28:25–33
6. Valckx FMJ, Thijssen JM. Characterization of echographic image texture by cooccurrence matrix parameter. *Ultrasound Med Biol* 1997; 23:559–571
7. Bleck JS, Ranft U, Gebel M, et al. Random field models in the textural analysis of ultrasound images of the liver. *IEEE Trans Med Imaging* 1996; 15:796–801
8. Cramblitt RM, Parker KJ. Generation of non-Rayleigh speckle distribution using marked regularity models. *IEEE Trans Ultrason Ferroelectr Freq Control* 1999; 46:867–874
9. Oelze ML, Zachary JF, O'Brien WD Jr. Characterization of tissue microstructure using ultrasonic backscatter: theory and technique for optimization using a Gaussian form factor. *J Acoust Soc Am* 2002; 112:1002–1011
10. Kikuchi T, Nakazawa T, Furukawa T, Higuchi T, Maruyama Y, Sato S. Quantitative estimation of the amount of fibrosis in the rat liver using fractal dimension of the shape of power spectrum. *Jpn J Appl Phys* 1995; 34:2831–2834
11. Shankar PM. Ultrasonic tissue characterization using a generalized Nakagami model. *IEEE Trans Ultrason Ferroelectr Freq Control* 2001; 48:1716–1720
12. Yamaguchi T, Hachiya H, Kamiyama N, Ikeda K, Moriyasu F. Estimation of characteristics of echo envelope using RF echo signal from the liver. *Jpn J Appl Phys* 2001; 40:3900–3904
13. Yamaguchi T, Hachiya H, Kamiyama N, Moriyasu F. Examination of the spatial correlation of statistics information in the ultrasonic echo from diseased liver. *Jpn J Appl Phys* 2002; 41:3585–3589
14. Yamada H, Ebara M, Yamaguchi T, et al. A pilot approach for quantitative assessment of liver fibrosis using ultrasound: preliminary results in 79 cases. *J Hepatol* 2006; 44:68–75
15. Desmet VJ, Gerber M, Hoofnagle JH, Manns M, Scheuer PJ. Classification of chronic hepatitis: diagnosis, grading and staging. *Hepatology* 1994; 19:1513–1520
16. Sandrin L, Fourquet B, Hasquenoph JM, et al. Transient elastography: a noninvasive method for assessment of hepatic fibrosis. *Ultrasound Med Biol* 2003; 29:1705–1713
17. Chen S, Fatemi M, Greenleaf JF. Quantifying elasticity and viscosity from measurement of shear wave speed dispersion. *J Acoust Soc Am* 2004; 115:2781–2785
18. Bercoff J, Tanter M, Fink M. Supersonic shear imaging: a new technique for soft tissue elasticity mapping. *IEEE Trans Ultrason Ferroelectr Freq Control* 2004; 51:396–409
19. Palmeri ML, Wang MH, Dahl JJ, Frinkley KD, Nightingale KR. Quantifying hepatic shear modulus in vivo using acoustic radiation force. *Ultrasound Med Biol* 2008; 34:546–558
20. Brusseau E, Kybic J, Deprez JF, Basset O. 2-D locally regularized tissue strain estimation from radio-frequency ultrasound images: theoretical developments and results on experimental data. *IEEE Trans Med Imaging* 2008; 27:145–160
21. Colletta C, Smirne C, Fabris C, et al. Value of two noninvasive methods to detect progression of fibrosis among HCV carriers with normal aminotransferases. *Hepatology* 2005; 42:838–845

消化器科，49(1)：69-78，2009　　49：69

特集II　C型慢性肝炎のペグインターフェロンとリバビリン療法の治療成績と投与の工夫

HCV genotype 1B・高ウイルス量症例におけるHCV Core・E1・NS5A領域の変異とインターフェロン/ペグインターフェロン＋リバビリンの反応性*

豊田秀徳**
熊田　卓**
桐山勢生**
谷川　誠**
久永康宏**
金森　明**
多田俊史**

Key Words：HCV genotype 1B, HCV protein, amino acid substitution, interferon sensitivity test, combination therapy with peginterferon and ribavirin

はじめに

C型慢性肝炎に対するペグインターフェロンとリバビリンの併用療法の登場によりその著効率は改善したが，難治性といわれるgenotype 1Bかつ高ウイルス量症例においては依然その著効率は50%前後である[1-3]．とりわけgenotype 1B・高ウイルス量症例の中にはペグインターフェロン・リバビリン治療中にも血中のC型肝炎ウイルスリボ核酸(HCV RNA)が消失せずnull-response(NR)となる抵抗例が存在する．これらペグインターフェロン・リバビリン療法に対する効果を規定するウイルス側の因子についてさまざまな検討がなされている．とりわけ，HCVにおけるアミノ酸の変異とインターフェロンを中心とした抗ウイルス療法の効果との関連については，いくつかの報告がされている[4-10]．榎本らがHCV NS5A領域の2,209～2,248番のアミノ酸，いわゆるISDRの配列とインターフェロン単独療法の効果との関連を報告[11]したのが1990年代後半であり，その後もいくつかHCVのアミノ酸変異とインターフェロン/ペグインターフェロン療法(およびリバビリンとの併用療法)の効果との関連が検討され，その結果が報告された[4-7,9,10]．

最近，芥田らはHCV core領域の70番および91番のアミノ酸配列がペグインターフェロン＋リバビリン併用療法の治療効果に強く関連していることを報告した[8]．HCV core領域70番および91番がともにmutant type(double mutant)である場合にはペグインターフェロン＋リバビリン併用療法におけるウイルス学的著効(sustained virologic response：SVR)率，すなわちHCVが排除される症例の割合が低いことが報告されている．さらに最近，DonlinらはHCV genotype 1Bの症例においてHCV core領域70番のアミノ酸変異に加え，E1領域139番のアミノ酸配列が治療効果に関連している可能性を報告した[7](表1)．

われわれは，現時点でのHCV genotype 1B・高ウイルス量のC型慢性肝炎症例に対するスタンダードな治療であるペグインターフェロン・リバビリン48週併用療法において，HCV core領域70番・91番およびNS5A領域2,209～2,248番のアミノ酸変異，加えてE1領域139番のアミノ酸変異についてインターフェロン投与に対するウイルスの反応性およびペグインターフェロン＋リバビリン併用療法の効果との関連を検証した．

---

* Association between amino acid substitution in HCV core, E1, and NS5A region and the response to the combination therapy with peginterferon and ribavirin.

** Hidenori TOYODA, M.D., Takashi KUMADA, M.D., Seiki KIRIYAMA, M.D., Makoto TANIKAWA, M.D., Yasuhiro HISANAGA, M.D., Akira KANAMORI, M.D. & Toshifumi TADA, M.D.: 大垣市民病院消化器科〔〒503-8502 大垣市浅頭町4-86〕；Department of Gastroenterology, Ogaki Municipal Hospital, Ogaki 503-8502, JAPAN

表1　過去の報告によるHCV genotype 1B症例のアミノ酸変異とインターフェロン療法の治療効果

HCV領域	アミノ酸	Good response	Poor response
Core	70	Arginine(Arg)	Glutamine(Gln)
Core	91	Leucine(Leu)	Methionine(Met)
E1	139	Threonine(Thr)	Alanine(Ala)
NS5A	2209～2248(ISDR)	intermediate/mutant	wild

表2　患者背景(n=107)

年齢(歳)	58.9±9.0
性別(男性/女性)	52(48.6)/55(51.4)
体重(kg)	59.1±10.2
インターフェロン治療歴(なし/あり)	65(60.7)/42(39.3)
輸血歴(なし/あり)	85(79.4)/22(20.6)
ALT(IU/l)	65.8±64.9
AST(IU/l)	55.9±44.3
γ-GTP(IU)	53.7±53.6
ALP(IU/l)	265.2±86.4
ALB(g/dl)	4.14±0.35
T-Bil(mg/dl)	0.69±0.28
白血球数(/μl)	5201±1197
ヘモグロビン(g/dl)	14.0±1.4
血小板数(X 10^4/μl)	16.6±5.1
肝組織像-activity(A0/A1/A2/A3)*	2(2.0)/55(53.9)/36(35.3)/9(8.8)
肝組織像-fibrosis(F0/F1/F2/F3)*	5(4.9)/61(59.8)/24(23.5)/12(11.8)
治療前HCV RNA(KIU/ml)	1760±1139
ペグインターフェロン減量	29(27.1)
リバビリン減量	49(45.8)
治療効果(SVR/relapse/NR)	39(36.5)/38(35.5)/30(28.0)

( )内は%．*5例は肝生検せず．

対象と方法

ペグインターフェロンα2bとリバビリンの48週投与を施行したHCV genotype 1Bかつ高ウイルス量(amplicor monitor法，version 2.0にて100 KIU/ml以上)の症例107例(男性52例：女性55例，年齢58.9歳)を対象とした．対象症例の臨床背景を表2に示す．42例(39.3%)が再投与症例であったが，ペグインターフェロン・リバビリン併用療法については全例初回投与であった．治療前HCV RNA量は1760±1139　KIU/mlであった．治療前に肝生検を施行した102例ではF0：5例(4.9%)，F1：61例(59.8%)，F2：24例(23.5%)，F3：12例(11.8%)であった．

HCVの各対象領域(Core領域・E1領域・NS5A領域)をシークエンスして70番・91番・139番・2,209～2,248番の各アミノ酸配列を決定した．全例でペグインターフェロン・リバビリン併用療法開始前に通常のインターフェロンa 2bの600万単位を単回投与して24時間後のウイルス量の変化を解析し(インターフェロン感受性試験：図1)，各領域の変異によりウイルス量の低下率を比較した．また，ペグインターフェロン＋リバビリン併用療法開始24時間後の治療前と比較したウイルス量の変化，および治療開始後4週目までの血中HCV RNAの陰性化(rapid virologic response：RVR)・治療開始後12週目までの血中HCV RNAの陰性化(early virologic response：EVR)・SVRの割合について各領域の変異ごとに比較した．なお，ペグインターフェロンおよびリバビリンの投与量，減量基準は規定の基準にのっとって行った．また今回の検討ではHCV RNAの定量はamplicor monitor法(version 2.0)にて，陰性化の判定はamplicor定性法にて行った．